Preparation and study of composites based on poly(3,4-ethylenedioxythiophene)

Master's Thesis

Materials Science MSc

Levente JUHÁSZ

Thesis Advisors:

Zsélyné Dr. Mária UJVÁRI

Prof. Dr. Győző LÁNG

Eötvös Loránd University

Faculty of Science

Institute of Chemistry

Laboratory of Electrochemistry and Electroanalytical Chemistry

Budapest, 2018.

Foreword

I would like to express my deepest gratitude to my advisor, *Prof. Dr. Győző Láng* who invited me to his research group and helped my work by professional advice.

I am also very grateful to my other advisor, *Dr. Mária Ujvári* who provided me with continuous inspiration and guidance during my work, and introduced me to electrochemical measurements.

The valuable support and advice of my laboratory fellows, *Dóra Zalka*, *Krisztina Szekeres* and *Noémi Kovács* is also acknowledged with appreciation.

I would like to acknowledge my appreciation to the staff of the Scanning Electron Miscroscope, *Dr. Zoltán Dankházi*, *Dr. Gábor Varga*, *Ádám Vida* and *Zsolt Maksa*, for carrying out the scanning electron microscopy measurements.

Last but not least I am also very grateful to my friends and family, for their support during my work.

Table of contents

List of abbreviations

Au:	Gold
CV:	Cyclic voltammetry
EDOT:	3,4-ethylenedioxythiophene
EDX:	Energy-Dispersive X-ray Spectroscopy
EIS:	Electrochemical Impedance Spectroscopy
ETD:	Everhart-Thornley detector
GO/rGO:	Graphene oxide / Reduced graphene oxide
GC/GCE:	Glassy carbon electrode
MSE:	Mercury / mercurous sulfate electrode
OCP:	Open circuit potential
PANI:	Polyaniline
Pd:	Palladium
PEDOT:	Poly(3,4-ethylenedioxythiophene)
PET:	Polyethylene terephthalate
PSS:	Polystyrene sulfonate
Pt:	Platinum
PTCNQ:	Poly(tetracyanoquinodimethane)
RDE:	Rotating disk electrode
SCE:	Saturated calomel electrode
SSCE:	Sodium chloride saturated calomel electrode
SEM:	Scanning Electron Mictroscopy
SHE:	Standard hydrogen electrode
XPS:	X-ray Photoelectron Spectroscopy

1. Introduction

The first extensively studied electrically conducting polymer was polyacetylene, whose discovery in 1977 is often referred to as the beginning of the modern history of conducting polymers [1]. The pioneering work of Alan J. Heeger, Hideki Shirakawa and Alan G. MacDiarmid was honoured by a Nobel-prize in 2000 for the discovery of the simplest conjugated conducting polymer, a halogen-doped, highly conductive polyacetylene [2]. Although polyacetylene has never found widespread industrial applications because of its unstable conjugated π-bonds (if unstabilized), this discovery led us to the fact that conducting polymers are of huge scientific interest these days.

However, the story of conducting polymers began in its widest sense already in 1862, when Henry Letheby successfully electropolymerized aniline during his investigations after a series of fatal poisonings in a hospital [3]. Later in the 1910s Willstätter intensively studied the oxidation states of aniline oligomers, although the complete description of the structure and the idea of a possible industrialisation of polyaniline (PANI) as a conducting polymer was only realised in the late 1960s [2]. Since then, polyaniline has been widely used in a plethora of industrial applications, even if its intesive colour (dependent on oxidation states) excludes uses where a transparent or light surface is needed.

The next important milestone in the history of conducting polymers was the discovery of polypyrrole in 1974 [4], followed by the intensive research on polythiophenes since the end of the 1960s [5]. Tourillon and Garnier succeeded in reaching a conductivity of 10-100 S/cm with perchlorate- and tetrafluoroborate-doped polythiophenes [6], although industrialisation again could not be attained due to instability in air and difficult processability. The discovery of poly(3,4-ethylenedioxythiophene) came in 1988 by the scientists of Bayer AG. in Leverkusen, Germany [2]. Stability issues have been eliminated both for PANI and PEDOT, what is for the most part due to the stabilisation effect of nitrogen and sulphur heteroatoms in the congjugated system.

After its discovery, companies Bayer, Starck and H.C. Starck Clevios started intensive research on PEDOT which has resulted in today's wide range of industrial applications [7]. Between 1989 and 2005 the number of scientific papers published on PEDOT increased exponentially, and although this trend has settled ever since, it must be seen that PEDOT is still intensively researched by scientists.

Today PEDOT stands in the limelight of science for the variety of its feasible composite materials. Possible composite materials are for instance noble metals, which catalyse many chemical or electrochemical reactions. My aim in this thesis is to give insight into the electrochemistry of palladium and platinum composites of PEDOT. Both the preparation and the study of PEDOT – palladium and PEDOT – platinum composites are going to be in the centre of interest.

2. Theoretical part

In this chapter, I am going to offer a brief survey of conducting polymers, especially of PEDOT. Also, I am going to introduce palladium and platinum composites based on PEDOT. Later, I am going to discuss the oxygen reduction reaction which is an important means for the study of noble metal composites.

2.1. Conducting polymers

Electrochemically active or conducting polymers consist of organic macromolecules which themselves are electrically conductive. At the first try we can classify them into two separate categories: ion (proton)- and electron-conducting polymers. Electron-conducting polymers can be divided into further classes according to the charge propagation within the polymer: redox polymers and electronically conducting (intrinsically conducting) polymers [8].

1) Redox polymers

The conduction of redox polymers is based on redox sites which are either covalently attached to the chain or held by electrostatic binding. Redox sites can be oxidized or reduced, thus electron-hopping can be realised between adjacent redox sites.

We can divide redox polymers into further classes according to whether the redox site is built into the chain or is in a pendant group. These covalently attached groups are mostly of organic or organometallic nature. Examples for redox polymers with covalently attached redox sites are poly(tetracyanoquinodimethanes) (PTCNQ), polyviologens (N,N-alkylated bipyridine-based polymers) or quinone polymers [8].

If a redox site is not covalently but electrostatically bound, the macromolecule is called an ion-exchange polymer or polyelectrolyte. These polymers are usually applied to the surface of an electrode and their counterions are exchanged to redox-active ions (e.g. for an appropriate cation for cation-exchange polymers). The electrostatically bound counterions (of small size) are more or less mobile within the polymer layer, however, polyelectrolyte counterions are practically fixed in the surface layer. Examples for redox polymers with electrostatically attached redox sites are Nafion (perfluorinated sulfonic acids), polystyrene sulfonate (PSS), or poly(4-vinylpyridine).

2) Electronically conductive polymers

Electronically conducting polymers contain conjugated double bonds and/or aromatic rings where positive holes can be introduced by way of so-called doping. The conductivity of such polymers increases to a large extent when doped [9, 10]. The delocalized electron system accounts for the charge propagation within the polymer chains, which is considerably supported by positive holes introduced. Interchain charge propagation is supposed to take place through electron hopping [8]. Examples for electronically conductive polymers are polyacetylenes, polypyrroles, polyanilines and polythiophenes.

Conducting polymers simultaneously merge the advantageous features of polymers and metals: they are easily processable, have excellent optical and mechanical properties and are lightweight, besides, they possess electrical characteristics similar to metals [11, 12, 13] and [14]. Moreover, they have the advantage that their chemical and physical properties can be widely tuned, they can be tailored to meet special requirements, even biologial or medical uses are feasible [15].

In the next section, one of the most actively researched conducting polymers, poly(3,4-ethylenedioxythiophene) i.e. PEDOT is going to be discussed.

2.2. Poly(3,4-ethylenedioxythiophene) (PEDOT)

The most common representative of electronically conductive polythiophenes is poly(3,4-ethylenedioxythiophene) i.e. PEDOT. PEDOT is made up of thiophene units, where the 3. and 4. atomic positions are linked by an ethylenedioxide-bridge. Also, there are intramolecular interactions between the oxygen and sulphur atoms of adjacent repeating units, what results in a rigid, unrotatable structure of the polymer chain. The structural formula of PEDOT can be seen in *Fig. 1.*:

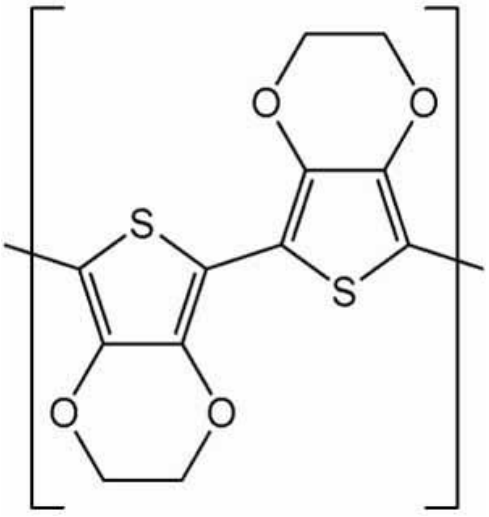

Fig. 1: Structural formula of PEDOT [16].

PEDOT is a widespread and extensively used conducting polymer as it is stable in air, easily processable, it has an average band gap and a relatively low redox potential (PEDOT/PEDOT$^{+\cdot}$, 0.1 V vs. SHE) [17]. Its has a disadvantage of poor solubility in water, hence it is often used in a coordination complex form with a counterion, mostly with the polymer polystyrene sulfonate (PSS).

2.2.1. Preparation of PEDOT films

1) Surface polymerization

Appropriate conducting films can be prepared from PEDOT:PSS, however, PSS is prone to absorb a significant amount of water which may cause corrosion for instance in electronic devices [18]. As an alternative, Li and Ma prepared a PEDOT layer without PSS: they immersed a PET substrate into a solution of iron-p-toluenesulfonate in butanol, then after applying a short drying phase, the film was immersed into an EDOT solution in cyclohexane [19]. Polymerization takes place only at the surface of the pretreated PET substrate where the iron-p-toluenesulfonate layer oxidizes EDOT.

2) Spin coating

In spite of the issues of PSS, spin coating of PEDOT:PSS dispersions is still one of the most frequently used techniques to prepare PEDOT layers [20], [21] and [22]. During this technique commercially available dispersions of PEDOT:PSS (e.g. Heraeus Clevios, AGFA, Sigma-Aldrich stb.) are poured on a rotating substrate, and a smooth, even surface can be obtained owing to the rotation.

3) *Vapour phase polymerization*

Vapour phase polymerization is a rarely used technique, however, it is suitable for preparing PEDOT films of high conductivity [23]. Kim placed a PET-substrate treated with iron-tosylate into EDOT atmosphere in an autoclave, what resulted in a coherent PEDOT layer on the substrate [24]. Disadvantage of this technique is the limitation of the size of substrates as an autoclave must be used [19].

4) Electropolymerization

Besides spin coating, the other most frequently used technique to prepare PEDOT films is electropolymerization, where the polymerization reaction is triggered and controlled by a potential or current program and it usually takes place in a three-electrode cell. Electropolymerization is a preferred technique for conducting polymer coatings because it is considerably reproducible and easy to control by the charge passed through the electrodes, thus well-defined composition, structure and thickness can be obtained [25].

Electropolymerization techniques can be classified into three main classes: galvanostatic, potentiostatic and potentiodynamic methods.

a) Galvanostatic electropolymerization

The current density between the working and the counter electrode is held constant during galvanostatic electropolymerization, what is often the best way to obtain a homogenic polymer layer on a substrate. Patra et al. found that galvanostatic electropolymerization of EDOT results in cauliflower-like structures with globular morphology. With increased current densities morphology tends to transform into a more porous, spongy structure. [26]

b) Potentiostatic electropolymerization

During potentiostatic electropolymerization the potential of the working electrode is held constant, and current-time curves can be registered. Similarly to galvanostatic electropolymerization, if EDOT is polymerized potentiostatically, the globular structure of the polymer transforms into a porous, sponge-like one with the increase of the applied potential [26].

c) Potentiodynamic electropolymerization

Potentiodynamic electropolymerization is considerably similar to cyclic voltammetry, where a triangle potential sign is applied to the working electrode and the current response is measured. Advantage of this technique is that the amplitude and cycling speed (frequency) may be unrestrictedly chosen therefore electropolymerization parameters can be tuned in a wide range.

2.2.2. Structure of PEDOT films

Polymers tend to form less ordered crystals than e.g. metals do: polymer chains are of varied length and conformation, chain imperfections may be present, too. There are crystalline regions in a polymer (so-called crystallites), however, no long-range order can be found, even the so-called “crystalline polymers” are not entirely crystalline. Thus, there is always an amorphous phase present within the polymer, which is dependent on the type of the polymer and the conditions of crystallization: whereas the degree of crystallinity can reach up to 80-90 % for polyacetylene [27], it is only 50 % for polypyrrole [7]. Crystallinity is usually

considerably hindered for PEDOT films as well. Although a paracrystalline structure might be detected for some PEDOT-tosylates [28], crystallography studies of PEDOT:PSS usually show no sign of crystallinity.

In potentiostatic and galvanostatic preparation routes huge polymer aggregates or islands start to form on the electrode surface, which then continuously grow during the electropolymerization, and a cauliflower-like film structure takes shape. In potentiodynamic conditions a more uniform film is deposited according to Castagnola [25]. The roughness of the polymer surface is a few hundred nanometers, however, it mostly depends on the film thickness. The stucture of the polymer layer is also influenced by the surface roughness of the (e.g. gold) substrate, as polymer aggregates tend to nucleate on surface defects, for instance scratches on the electrode

2.3. Composites of PEDOT

PEDOT has proved to form excellent transparent conducting films, therefore it had its first industrial use as an antistatic coating in photography [29]. Since then, PEDOT and its composites have been widely used in applications like supercapacitors, integrated circuits, touchscreens, OLEDs or solar cells.

A separate branch of applications makes use of the electrocatalytic properties of the composites of PEDOT. These materials are mostly composites of noble metals which are excellent catalysts, however, they are expensive, rigid and as their catalytic reactions mainly take place on their surface, it would be advantageous to find a proper „substrate" material which they could be embedded in. If we could merge the advantages of noble metals and the advantageous features of PEDOT, as easy processibility, excellent mechanical properties, decent conductivity and low price, we could prepare composites for a wide range of applications. In the forthcoming paragraphs, two noble metal composites of PEDOT, PEDOT – palladium and PEDOT – platinum composites are going to be discussed.

2.3.1. PEDOT – palladium composites

Palladium composites are among the most widely studied PEDOT based composites. Their uniqueness is mainly due to their advantageous catalytic properties, a few examples for them are hydrogen peroxide sensing [30, 31], electrooxidation of hydrazine [32], ethanol [33] or propanediol [34]; glucose- [35, 36] and ammonia-sensors [37] or the electrocatalytic oxygen reduction reaction [38].

There are several ways to prepare PEDOT-palladium composites, both the PEDOT and the palladium phase can be obtained by various techniques. The polymer phase is usually prepared by electropolymerization [39], polymerization with chemical oxidation [33] or by drop-coating from a PEDOT:PSS dispersion [40]. The palladium phase is mostly prepared by immersing the PEDOT phase into a palladium-containg solution [41, 30]. However, there is also a possible route to prepare the PEDOT and the palladium phase simultaneously, using palladium as an oxidizing agent for EDOT [31, 42].

Electropolymerization of PEDOT can be carried out galvanostatically [43], potentiostatically [44] or potentiodynamically [36], the structure and the thickness of the film vary according to the preparation route used. The concentration of the EDOT solution for electropolymerization is usually 0.01 M [42] or 0.05 M [45], the conducting salt added is mostly Na_2SO_4 or $LiClO_4$.

Before the immersion, the PEDOT film usually undergoes a reduction phase where it is held on a negative potential (compared to its standard potential) to regain its reducing capacity. Time and potential of reduction are varied in the literature, ranging from 120 s [45] to 1200 s [44], and from -1.4 V (vs. MSE) [44] to -0.2 V (vs. AgCl-electrode in sat. NaCl) [43]. The reduction phase often takes place in a solution of 0.1 M H_2SO_4 [41].

Immersion takes place usually in ($5 \cdot 10^{-3}$ – $5 \cdot 10^{-4}$) M $PdCl_2$ – 0.1 M H_2SO_4 solution [41, 43] or in $2 \cdot 10^{-3}$ M $PdSO_4$ – 0.5 M H_2SO_4 solution [44]. One of the most important parameters of the immersion is whether it is carried out in an electroless way. Eliseeva [43, 46] and Kondratiev [41] deposited palladium onto PEDOT films electrolessly, Ilieva also only measured the open circuit potential (OCP) during the deposition of palladium [44]. However, Harish et al. applied -0.1 V (vs. MSE) on the working electrode for 360s during the deposition of palladium [47]. Dash and Munichandraiah carried out the electrodeposition of palladium at a constant potential of 0.1 V (vs. SCE) and at 0.0 V (vs. SCE), too [48].

Another feasible electrochemical method was used by Santhosh et al. who performed the electrodeposition and stripping of palladium at a scan rate of 100 mV/s in a potential range of -1.6 V to 1.1 V (vs. Ag/AgCl electrode). Reduction and oxidation peaks of palladium appeared at -0.5 V and 0.25 V (vs. Ag/AgCl electrode), respectively [36]. Time of the immersion is also considerably varied in literature, ranging between 30-180 s [30] or 60-300 s [39], however, immersion time is often not mentioned in scientific papers.

The structure of PEDOT-palladium composites depends to a great extent on the substrate electrode (glassy carbon [41, 44], carbon paper [34, 48] etc.) and the deposition conditions. Palladium tends to form small particles not only on the surface of the polymer but also within its pores which are accessible for the electrolyte [39]. Kondratiev also found that palladium particles preferably grew on larger PEDOT aggregates [41], therefore palladium is not evenly distributed on the polymer surface. According to Dash and Munichandraiah, the nucleation of palladium takes place preferably on high-energy surface sites of the polymer, i.e. crystal edges, kinks or other defects act as nucleation sites for the palladium crystals [34]. The latter authors prepared a PEDOT-palladium composite on carbon paper, where palladium formed tree-like 3D structures which grew perpendicular to the substrate [34].

2.3.2. PEDOT – platinum composites

Platinum-containing PEDOT-based composites are (like PEDOT-palladium ones) in the centre of interest due to their special electrocatalytic properties. The research of PEDOT – platinum composites is focused overwhelmingly on direct methanol fuel cells (DMFC) [49, 50], in which PEDOT acts as a support material for the methanol oxidation electrocatalyst. Other applications span solar cells [51], electrooxidation of formic acid [52, 53] or hydrogen peroxide sensors [54].

Similarly to PEDOT-palladium composites, PEDOT-platinum composites can be obtained through a wide range of techniques. The PEDOT phase can be prepared by electropolymerization [52], spin-coating [55], chemical oxidation [49, 50] or by a photo-assisted chemical method for the simultaneous deposition of both the PEDOT and the platinum phases [54]. The deposition of platinum nanoparticles is often carried out electrochemically, usually at a constant potential of 0.1 V (vs. SCE) [52, 56] in (0.002-0.005) M H_2PtCl_6 – 0.1 M H_2SO_4 solution. However, Wu et al. applied a potential of -0.2 V (vs. Ag/AgCl electrode) in 0.01 M HCl – 0.1 M KCl – 0.005 M H_2PtCl_6 solution [55], and Yue et al. carried out platinum

deposition at -0.2 V (vs. SCE) in 0.5 M H_2SO_4 – 0.003 M H_2PtCl_6 solution [57]. Tsai used cyclic voltammetry to electrodeposit platinum on an ITO/PEDOT substrate [51]. Contrary to PEDOT/palladium composites, usually no reduction phase is applied to PEDOT prior to platinum deposition. The deposition times of platinum are mostly not mentioned in the papers.

The stucture of PEDOT/platinum composites depends to a considerable extent on the substrates and the morphology of the PEDOT layer. Wu et al. prepared PEDOT:PSS – platinum composites where platinum formed spheres of a size of 100-300 nm [55]. XPS studies confirmed that platinum spheres don't aggregate due to the stabilisation effect of SO_3^- -groups in PSS. Dash et. al also found uniformly distibuted platinum spheres during SEM studies of PEDOT-platinum composites [52]. When deposited on bare carbon paper electrode (in the absence of PEDOT), platinum spheres had a less uniform distribution on the surface and grew larger in size. Besides, higher deposition charges resulted in larger platinum spheres (200-400 nm) and platinum clusters even merged to a homogeneous film above 1 C/ cm^2 charge density. The idea that PEDOT facilitates the nucleation of platinum was confirmed also by Patra and Munichandraiah [56].

2.3.3. Oxygen reduction reaction (ORR)

Fuel cells involve the oxidation of chemical fuels on the anode and the reduction of oxygen (oxygen reduction reaction, ORR) on the cathode. The cathodic reaction i.e the oxygen reduction reaction is kinetically slow as it comprises several complex processes e.g. proton and electron transfer or oxygen-bond breaking [58].

The oxygen reduction reaction can occur both in acidic and alkaline media where the two-electron transfer reactions are the following (possible four-electron transfer reactions are in brackets):

<u>Alkaline media:</u>

$$O_2 + H_2O + 2\,e^- \rightarrow HO_2^- + OH^- \quad (1)$$

$$H_2O + HO_2^- + 2\,e^- \rightarrow 3\,OH^- \quad (2)$$

$$(O_2 + 2\,H_2O + 4\,e^- \rightarrow 4\,OH^-) \quad (3)$$

Acidic media:

$$O_2 + 2\,H^+ + 2\,e^- \rightarrow H_2O_2 \quad (4)$$

$$H_2O_2 + 2\,H^+ + 2\,e^- \rightarrow 2\,H_2O \quad (5)$$

$$(O_2 + 4\,H^+ + 4\,e^- \rightarrow 2\,H_2O) \quad (6)$$

Currently, platinum-based composites are the most frequently used catalysts for the oxygen reduction reaction, however, platinum has disadvantageous properties as well. On the one hand, platinum is very expensive (a substantial amount of platinum is needed to accelerate the sluggish oxygen reduction reaction), on the other hand platinum tends to suffer from severe dissolution and migration issues during the electrochemical process [58].

Possible alternatives could be the alloying of platinum with nonprecious metals [59], however, these alloys are not always able to achieve both excellent ORR activity and durability at low cost. Recently, nanomaterials are in the centre of interest as possible candidates for ORR catalysts. Platinum-based nanorods, nanosheets, three-dimensional networks or other porous structures have attracted much attention for their excellent catalytic activity and durability [60]. Besides, these multidimensional platinum-based structures are generally less prone to dissolution and aggregation [58].

Catalyst supports are often used as a means to simultaneously reduce the amount of platinum needed and enhance the activity of the catalyst [61] and [62]. Other materials have been investigated as well to propose a less expensive alternative to platinum catalysts. For instance, Choe et al. prepared PEDOT functionalized graphene with palladium nanoparticles as a catalyst for the oxygen reduction reaction [38]. They found that the rGO/PEDOT/Pd composite had remarkable electrocatalytic activity and stability compared to rGO/Pd. Moreover, the Koutecky-Levich and Tafel analysis suggested that the oxygen reduction reaction mechanism took place as a direct four-electron transfer process [38].

The Levich equation is a beneficial tool for studying the oxygen reduction reaction as it describes the diffusion and slow flow conditions around a rotating disk electrode. The Levich equation can be expressed as the following:

$$I_L = (0.620) \cdot nFAD^{2/3}\omega^{1/2}\nu^{-1/6}C \quad (7)$$

where I_L is the Levich current, n is the number of moles of electrons transferred in the half reaction, F is the Faraday constant, A is the electrode area, D is the diffusion coefficient, ω is the angular rotation rate of the electrode, ν is the kinematic viscosity and C is the analyte concentration.

Thus, if the Levich current is plotted against the square root of the angular rotation rate, the presence of diffusion control in the electrochemical reaction can be determined.

3. Objectives of the thesis

As we have seen in the theoretic part, PEDOT-based noble metal composites are feasible electrocatalysts for a wide range of electrochemical reactions. However, there are still some unexplained questions about the preparation and the electrochemical properties of these systems.

The most appropriate route to prepare a PEDOT – palladium or PEDOT – platinum composite always depends on the given application and the desired properties of the electrocatalyst. If we could acquire, however, more knowledge on the effects of the conditions of e.g. reduction and deposition, we would be able to predict an appropriate preparation route in a more exact way. Another important point is that most scientific papers discuss preparations where surfactants or other additives are used, "pure" PEDOT – palladium or PEDOT – platinum composites are rarely prepared and studied. Besides, little information is found on the electrochemical impedance analysis of such composites.

This thesis can be divided into two main parts. The purpose of the first part is to study the effect of different preparation routes on the properties of PEDOT-palladium composites. Cyclic voltammetry and electrochemical impedance spectroscopy were used to characterise the electrochemistry of these composites. Furthermore, scanning electron microscopy was used to study the morphology and the palladium content of the samples.

The second part of this thesis is the study of a PEDOT-platinum composite. A common electrochemical preparation route was chosen to prepare a PEDOT-platinum composite on a platinum rotating disk electrode to study the electrocatalytic properties of the composite both in oxygen-free and oxygen-containing electrolyte.

4. Experimental part

4.1. Methods of investigation

4.1.1. Cyclic voltammetry

Cyclic voltammetry is one of the most common investigation methods of electrochemically active samples. This technique allows us to study the redox properties of a sample or the growth of film thickness with ease, furthermore, oxidation potentials and several kinetic parameters of a studied system can be determined [63].

Cyclic voltammetry is a technique where a triangle-shaped potential signal is applied to the working electrode, and the appropriate current response is measured. Cyclic voltammetry studies provide current-potential or current-time graphs, called voltammograms.

An idealised case of a voltammogram is when an electrochemically reversible behaviour prevails, i.e. charge transfer at interfaces and charge transport within the film are fast and no specific (attractive or repulsive) interactions between redox species are present. This may be the case for a thin polymer film on a substrate and/or at low scan rates. A scheme of an ideal reversible surface voltammogram can be seen in *Fig. 2.*:

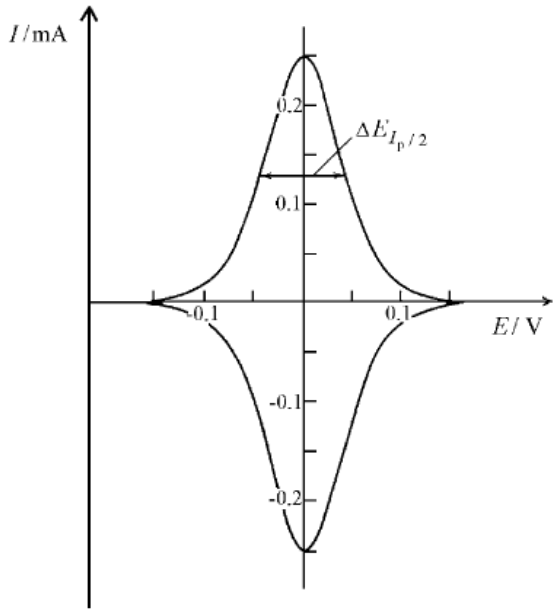

Fig. 2.: Scheme of an ideal reversible surface voltammogram [63].

The anodic and cathodic peak currents (I_{pa}, I_{pc}) of an ideal reversible surface voltammogram can be expressed by the following equation:

$$I_p = \frac{n^2 F^2 A \Gamma \nu}{4RT} \tag{8}$$

where I_p is the peak current, n is the number of charge transfer, F is the Faraday-constant, A is the electrode surface, Γ is the total surface concentration, v is the scan rate, R is the gas constant and T is the temperature.

The voltammogram will show a diffusional character if the charge transport within the film and/or the charge transfer at the interfaces are slow, i.e. the equilibrium condition doesn't prevail. The diffusional (or quasi-reversible) character of the voltammogram can be recognized by the shift of peak potentials and/or the diffusional tailing. A diffusional voltammogram can be seen in *Fig. 3.*:

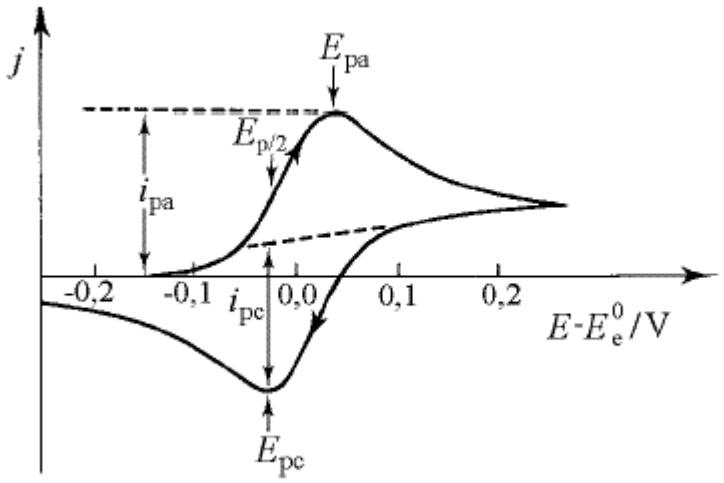

Fig. 3.: Scheme of a diffusional voltammogram of a reversible redox system [64].

E_{pa} and E_{pc} are the potentials of the anodic and cathodic peak currents, respectively. The peak currents of such a voltammogram are described by the Randles-Sevcik-equation:

$$I_p = 2.69 \cdot 10^5 \, n^{\frac{3}{2}} \cdot A \cdot D_i^{\frac{1}{2}} \cdot c_i^* \cdot \nu^{\frac{1}{2}} \tag{9}$$

where D_i is the diffusion coefficient and c_i^* is the concentration of the electrochemically active species.

As we will see later, however, neither of these cases (and equations) can describe a conducting polymer or its composite properly.

4.1.2. Electrochemical Impedance Spectroscopy

Electrochemical impedance spectroscopy is an important tool for electrochemical studies, especially when a description of the charge transport and charge transfer processes is required. It has the advantage (contrary to e.g cyclic voltammetry or chronoamperometry) that only a small-amplitude (<5 mV) sinusoidal voltage (or current) is applied to the working electrode, therefore the perturbation from equilibrium is negligible [65]. It implies that neither significant ion- and solvent transport nor morphology changes will be triggered during the measurement, thus the system can be studied approximately in its steady state.

The applied sinusoidal voltage (*U(t)*) and the current response (*I(t)*) can be expressed by the following equations:

$$U(t) = U_m sin(\omega t) \tag{10}$$

$$I(t) = I_m sin(\omega t + \varphi) \tag{11}$$

where U_m and I_m are the amplitudes of the voltage and the current signal, respectively, ω is the angular frequency of the perturbation, δ is the phase difference of the current response, and *t* is time.

The impedance (*Z*) of the electrochemical system can be expressed as following:

$$Z = U(t)/I(t) = |Z|exp(i\varphi) = Z' + iZ'' \tag{12}$$

where Z' and Z'' are the real and the imaginary parts of the impedance, respectively, and $i = \sqrt{-1}$.

A series of “theoretical” Argand-diagrams of the impedance function of a polymer-modified electrode is shown in *Fig. 4.*:

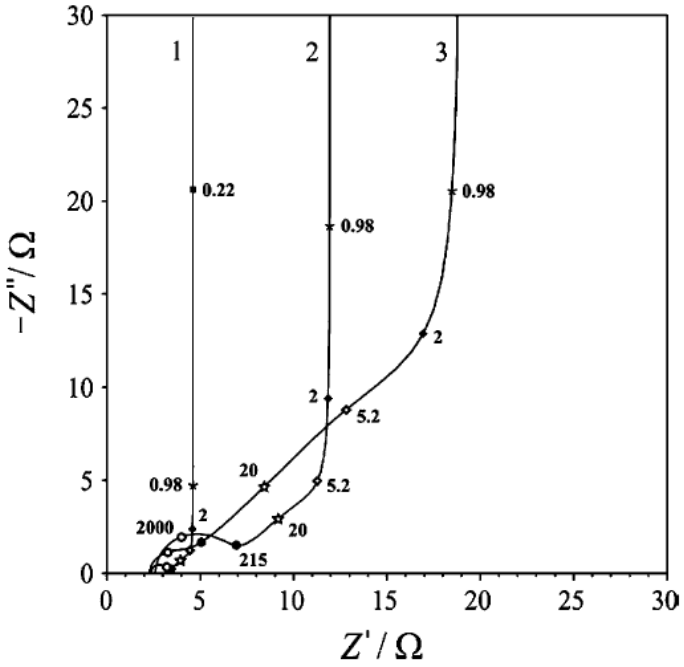

Fig. 4.: Argand diagram of “ideal” impedances of a polymer-modified electrode at different electrode potentials [66].
Effect of potential on impedance spectra.
Potentials of the impedance spectra: (1) E = 0.0 V, (2) E = 0.1 V and (3) E = - 0.1 V.
Small numbers indicate frequency values in Hz.

As we can see in *Fig. 4*, an ideal impedance spectrum consists of three main sections. The first one is the high frequency phase (characterized by a semicircle) which is related to the charge-transfer of the system. The linear section at medium frequencies is called Warburg phase and it is characteristic of the charge transport (diffusion) properties within the film. The third section is a nearly vertical linear section at low frequencies which describes the capacitive saturation of the polymer film. It is important to mention that a real impedance spectrum will not necessarily contain all these phases, it depends on the system under study and the measurement conditions which ones appear in the spectrum.

The proper evaluation of impedance spectra is mostly complicated, however, several parameters (e.g. solution and film resistance (R_s), charge transfer resistance (R_{ct}), Warburg-constant (σ) and double-layer capacitance (C_{dl})) can be estimated through graphical and numerical methods (see *Appendix*).

4.1.3. Scanning Electron Microscopy

Scanning electron microscopy is an indispensable tool in materials science as it provides a two-dimensional image of the surface of a sample with a (theoretic) lateral resolution of up to 1 nm [67]. In a scanning electron microscope (SEM) an electron beam scans the surface of the sample in high vacuum. The energy of the electron beam is usually between 500 eV-30 keV and it is focused to a spot with a diameter of a few nm. When the electron beam hits the surface of the sample, several interactions can take place: electrons can scatter on the surface elastically or inelastically, secondary electrons can emerge from the surface, X-ray radiaton or even Auger-electrons can be present. The emerging electrons and photons are detected by separate detectors in the vacuum chamber. Scanning electron microscopes use secondary electrons emerging from the sample to create an image of the surface. Backscattered electrons can be used as well for imaging, however, the available resolution is only 2-4 nm in this case. The energy of X-ray photons is dependent on the transition they come from, hence they can be used for chemical analysis.

4.2. Experimental conditions

Cyclic voltammetry and electrochemical impedance spectroscopy studies were carried out in 0.1 M H_2SO_4 saturated with argon (if not mentioned different) at room temperature. Before measurements, argon was bubbled through the electrolyte for 30 minutes to remove the oxygen in the cell. The three-electrode cell and other glass parts were soaked in Caro-acid ($n(H_2SO_4)$: $n(H_2O_2)$ = 1 : 1) for at least a day and washed carefully with Milli-Q water before measurements. Chloride ions were removed from glass parts by steam.

4.2.1. Preparation of PEDOT films

Working electrodes were polished with 0.25 μm diamond suspension on a velvet disk, then underwent an electrochemical cleaning phase using cyclic voltammetry (see *Appendix*). PEDOT films were prepared in a three-electrode cell in argon atmosphere, with saturated calomel electrode (SCE) as reference electode and a platinum wire as counter electrode. The electropolymerization was carried out galvanostatically, at a current density of j = 0.2 mA/cm^2

from a solution of 0.1 M Na_2SO_4 – 0.01 M EDOT. Electrode materials, surface areas (*A*) and electrodeposition times (*t*) are shown in *Table 1.*:

Sample	Electrode	*A* / cm^2	*t* / s
Pe1/Pd1	Au	1	1000
Pe2/Pd2	Au	2	3600
Pe3/Pd3	Au	2	3600
Pe4/Pd4	Au	2	3600
Pe5/Pt5	Pt (RDE)	0.19	3600

Table 1.: Details of PEDOT electrodeposition.
Pe1-4 denote Au | PEDOT systems and *Pe5* refers to a Pt | PEDOT system where the substrate is a platinum rotating disk electrode. *Pd1-4* denote Au | PEDOT | Pd composites, *Pt5* refers to a Pt | PEDOT | Pt composite.

4.2.2. Preparation of PEDOT – palladium and PEDOT – platinum composites

PEDOT films were immersed into solutions of palladium or platinum to prepare PEDOT – palladium and PEDOT – platinum composites. Immersions were carried out in a glass beaker with a glassy carbon auxiliary- and a saturated calomel reference electrode. In case of PEDOT – palladium composites, PEDOT films underwent a reduction phase before the immersion. Reduction and immersion conditions are shown in *Table 2.*:

Sample	Reduction			Immersion		
	Solution	(*E* vs. SSCE) / V	*t* / s	Solution	(*E* vs. SCE) / V	*t* / s
PEDOT – palladium composites						
Pd1	0.1 M H_2SO_4	-0.1	600	0.005 M $PdCl_2$ - 0.1 M H_2SO_4	0.1	150
Pd2	0.1 M H_2SO_4	-0.1	600	0.005 M $PdCl_2$ - 0.1 M H_2SO_4	0.1	150
Pd3	0.1 M H_2SO_4	-0.4	600	0.005 M $PdCl_2$ - 0.1 M H_2SO_4	-	300
Pd4	0.1 M H_2SO_4	-0.4	600	0.005 M $PdCl_2$ - 0.1 M H_2SO_4	-0.4	150
PEDOT – platinum composites						
*Pt5**				0.005 M H_2PtCl_6 - 0.1 M H_2SO_4	0.1	150

Table 2.: Conditions of the composite preparation.
E refers to the applied potential on the working electrode during the reduction and immersion step.
*The sample *Pt5* was immersed at a rotation rate of 150 rpm.

4.2.3. Study of PEDOT films and composites

Cyclic voltammetry and impedance measurements were carried out in a three-electrode cell with the polymer- /polymer-composite-modified electrode as the working electrode, a gold sheet as auxiliary electrode and a sodium chloride saturated calomel electrode (SSCE) as reference electrode. The reference electrode was connected to the solution phase within the electrochemical cell through a Luggin-capillary to ensure the electric connection of the reference electrode to the solution without significant ionic contamination from the reference electrode. The Luggin-capillary included a platinum wire connecting the solution phase and the reference electrode connection of the potentiostat directly via a condensator of 0.1 μF capacity. A scheme of the three-electrode cell can be seen in *Fig.5*.

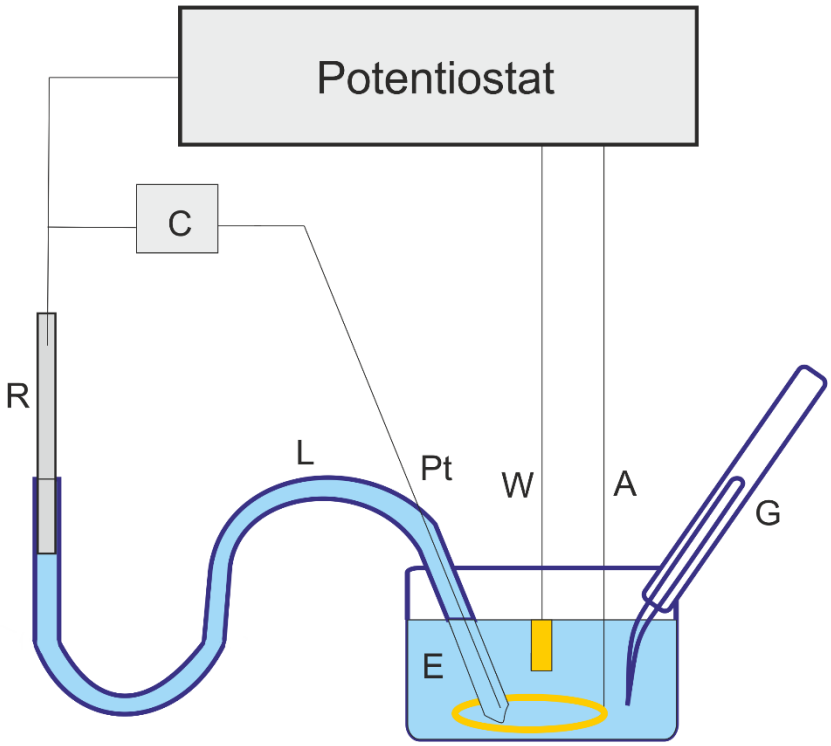

Fig. 5.: Scheme of the three-electrode cell.
R: reference electrode, W: working electrode, A: auxiliary electrode, L: Luggin-capillary, Pt: platinum wire, C: condensator, E: electrolyte, G: gas inlet.

Cyclic voltammograms were recorded at a scan rate of 100; 50; 20 and 10 mV/s. In figures, the 3. cycle is shown for the scan rates 100 mV/s and 50 mV/s, and the 2. cycle is shown in case of the scan rates 20 mV/s and 10 mV/s. Electrochemical impedance spectroscopy studies were made at potentials of E = (-0.2, 0.0, 0.2 and 0.4) V vs. SSCE and in a frequency range of 50 kHz – 7.5 mHz (100 kHz – 7.5 mHz in case of the platinum composite on a platinum rotating disk electrode (RDE)). Sinusoidal perturbation signals had an amplitude of 10 mV.

A Zahner IM6 potentiostat was used for the preparation and study of the PEDOT films and composites. A PINE MSR rotator system was used for the study of the oxygen reduction reaction. Scanning electron microscopy measurements were made using a FEI Quanta^{TM} 3D high-resolution, low pressure SEM instrument. Images were taken with secondary and backscattered electrons detected by an Everhart-Thornley detector (ETD) and a low-kV high contrast vCD detector. Energy-dispersive X-ray analysis (EDX) was made to measure the palladium content of the PEDOT – palladium composite samples.

5. Results and discussion

5.1. Study of PEDOT films

5.1.1. Electropolymerization of PEDOT

An electrode potential vs. time plot recorded during the electropolymerization of a PEDOT film on a gold substrate can be seen in *Fig. 6.*:

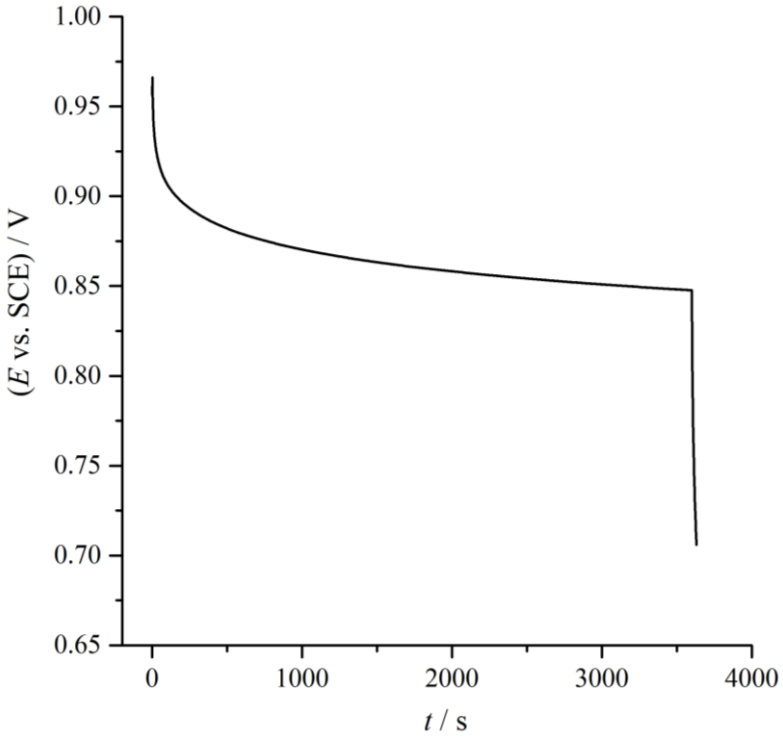

Fig. 6.: Galvanostatic electropolymerization of Au | PEDOT sample *Pe2*.
j = 0.2 mA / cm^2, t = 3600 s, A = 2 cm^2.

As we can see in *Fig.6.*, the electrode potential drops considerably at the beginning of the process, indicating the start of the electropolymerization.

5.1.2. Cyclic voltammetry

Cyclic voltammograms recorded on the PEDOT film *Pe2* are shown in *Fig. 7.*:

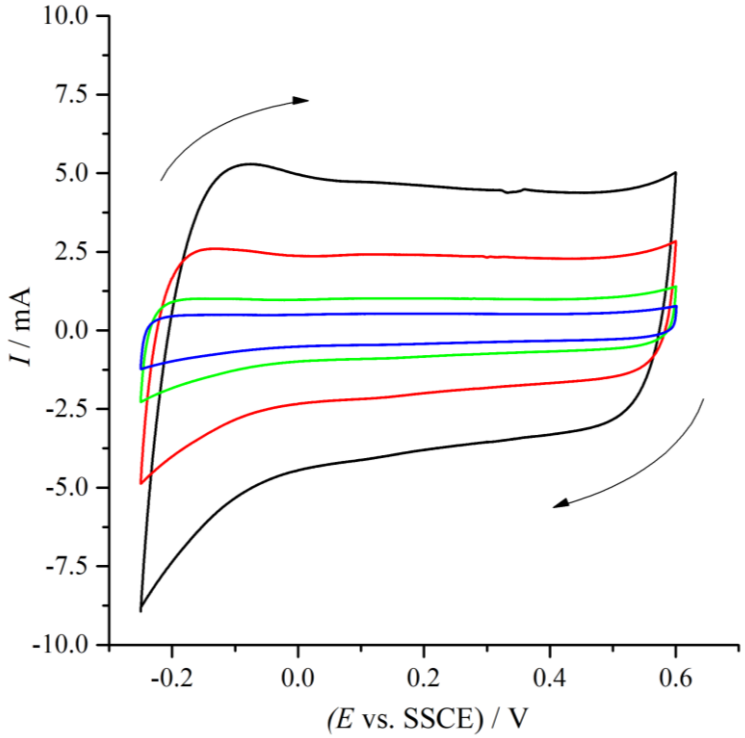

Fig. 7.: Cyclic voltammograms of Au | PEDOT sample *Pe2* in 0.1 M H_2SO_4.
Potential range: (E = -0.25 – +0.6 V) vs. SSCE.
Scan rates: 100 (▬); 50 (▬); 20 (▬); 10 (▬) mV/s.

As it can be seen in *Fig. 7.*, there is significant difference between the anodic and cathodic currents at a given potential, indicating the capacitive character of the PEDOT layer. Besides, currents increase with higher scan rates, as expected.

5.1.3. Electrochemical Impedance Spectroscopy

Impedance measurements were made at potentials of E = (-0.2, 0.0, 0.2 and 0.4) V vs. SSCE in a solution of 0.1 M H_2SO_4. As the inductivity arising from the experimental setup was not negligible, corrections were made to the spectra (see *Appendix*). Impedance spectra of the PEDOT sample *Pe2* can be seen in *Fig. 8.*:

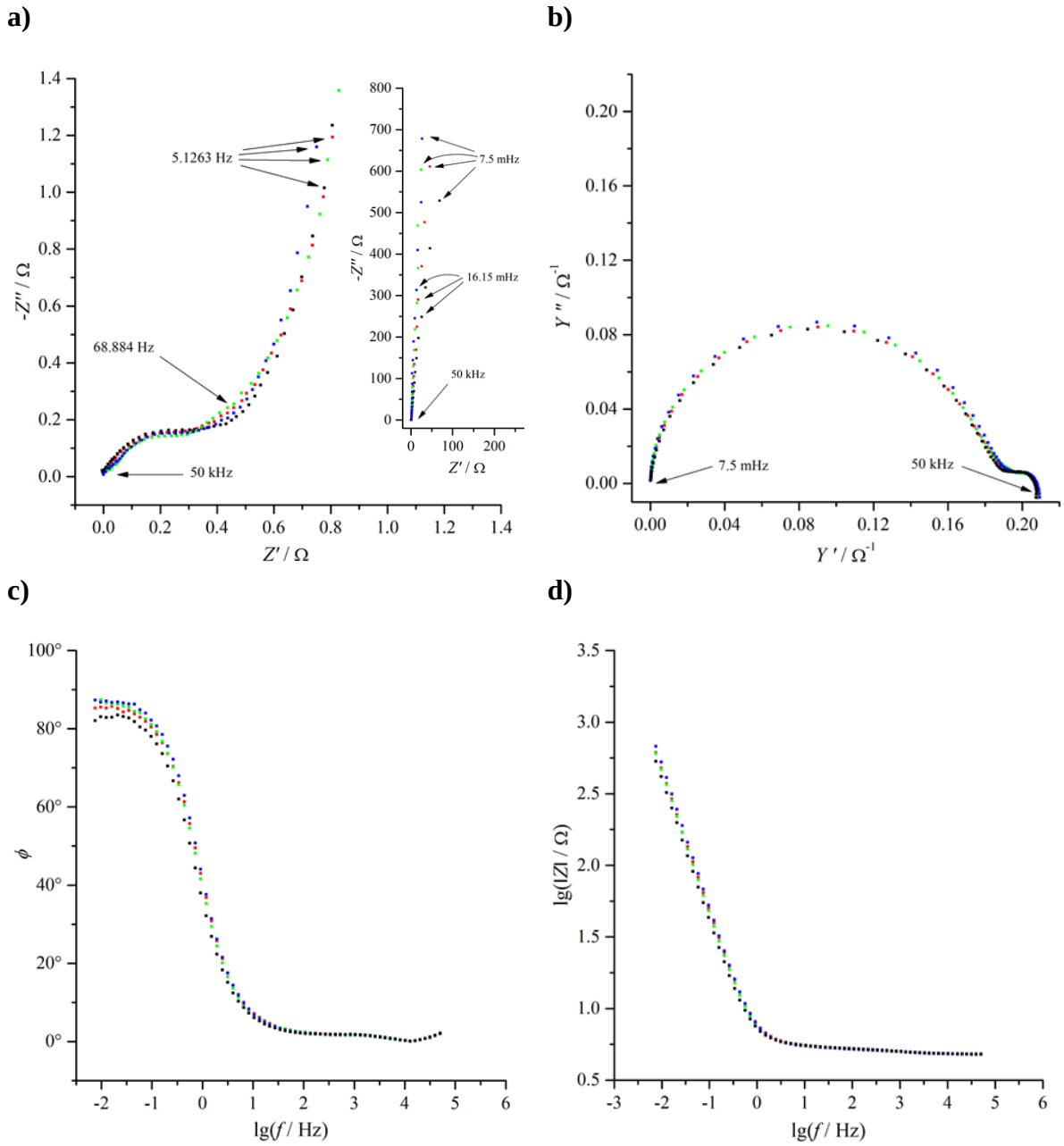

Fig. 8.: Impedance spectra of the Au | PEDOT sample *Pe2* in 0.1 M H_2SO_4.
Electrode potentials: -0.2 (■); 0.0 (■); 0.2 (■); 0.4 (■) V vs. SSCE.
a) Argand diagrams of the high frequency range and the whole spectra (*Z* ' and *Z* '' denoting the real and the imaginary parts of the impedance, respectively); **b)** the imaginary part (*Y* '') of the admittance as a function of the real part (*Y* ') of the admittance; **c)** phase angle as a function of $\lg\tilde{f}$; **d)** $\lg|\tilde{Z}|$ as a function of $\lg\tilde{f}$ ($|\tilde{Z}|$is the modulus of the impedance). ~ signs denote the magnitude of quantities.

In the Argand diagrams (*Fig. 8.* **a)**) we can see semicircles at high frequencies that are characteristic for the charge transfer. The Warburg section is quite indistinct at medium frequencies but the spectra show definite capacitive saturation at low frequencies. It is also important to add that spectra of different potentials coincide to a great extent, implying that the potential dependence of the impedance is quite small for this system. In the Bode plot (*Fig. 8.* **c)**) the phase angles tend towards 90° at small frequencies implying that capacitive behaviour prevails, and also, that there is no other process taking place in this frequency range.

5.2. Study of PEDOT – palladium composites

5.2.1. Cyclic voltammetry

PEDOT – palladium composites of different preparation routes were studied by cyclic voltammetry to be able to compare their electrochemcial behaviour to that of the "pure" PEDOT samples. Cyclic voltammograms of PEDOT and PEDOT – palladium composites in 0.1 M H_2SO_4 can be seen in Fig. *9.*. As we can see in the figure, there are no significant differences between voltammograms of an individual PEDOT and the respective composite sample in this potential range. Voltammograms of samples of different preparation do not differ significantly, either. Currents at the same scan rates look rather alike, the rectangular shapes of voltammograms indicate a capacitive character of the composite, similarly to PEDOT.

At more negative potentials, hydrogen evolution takes place, as it can be seen in Fig. *10.*. The voltammograms of the composite samples (both *Pd3* and *Pd4*) show well pronounced reduction peaks at the negative end of the potential range (E = - 0.5 V vs. SSCE) which are a clear sign of hydrogen evolution. On the contrary, hydrogen reduction peaks cannot be found in the voltammograms of PEDOT samples in this potential range, implying that the catalytic character of the added palladium accounts for the enhanced hydrogen evolution. The comparison of the reduction peaks suggests that the composite sample *Pd4* catalyses the hydrogen reduction more efficiently than the sample *Pd3*.

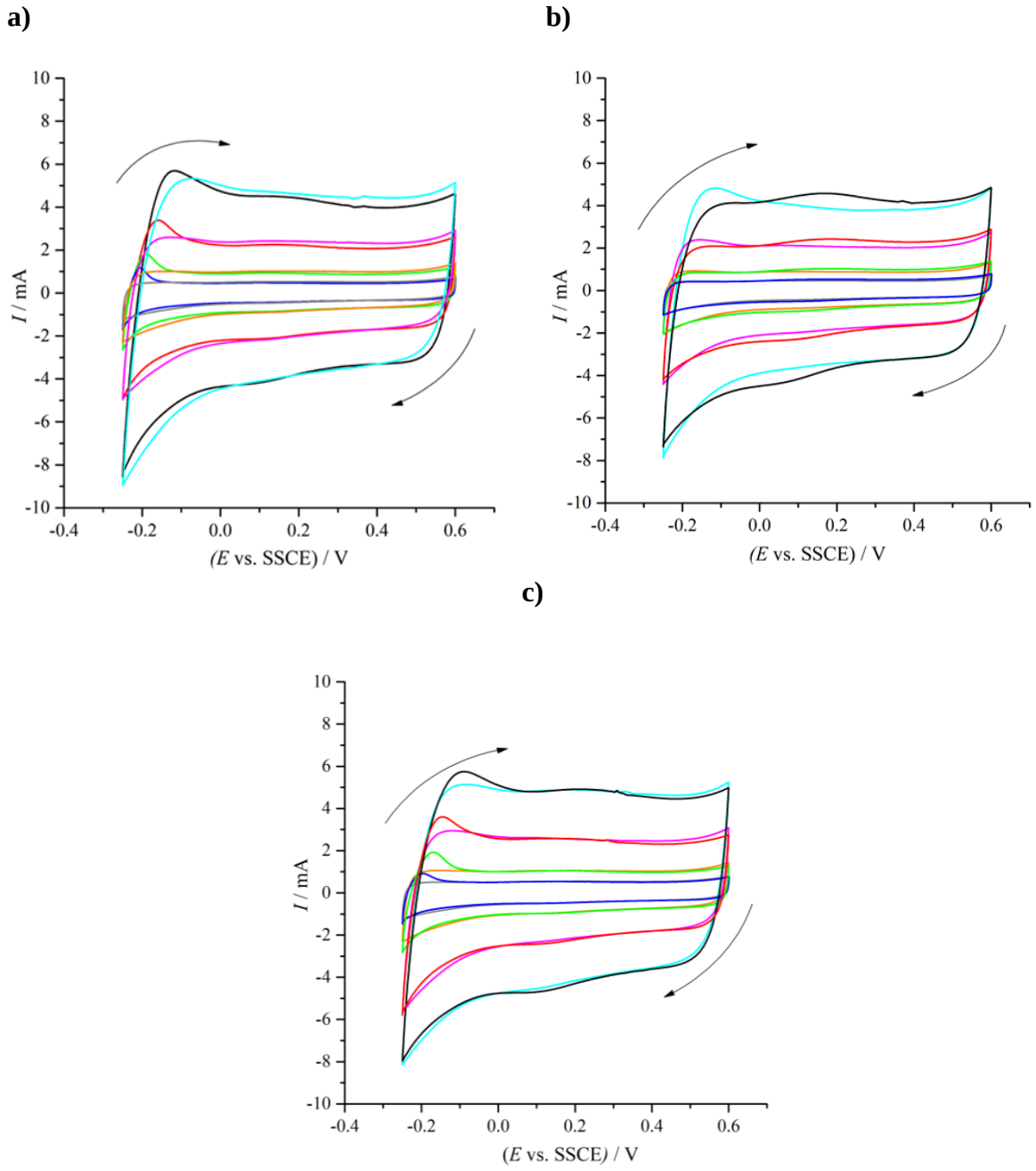

Fig. 9.: Cyclic voltammograms of Au | PEDOT and Au | PEDOT | Pd samples in 0.1 M H_2SO_4.
Potential range: (E = -0.25 – +0.6 V) vs. SSCE.
Scan rates: 100 ( ); 50 ( ); 20 ( ); 10 ( ) mV/s for Au | PEDOT and 100 ( ); 50 ( ); 20 ( ); 10 ( ) mV/s for Au | PEDOT | Pd samples.
a) *Pe2* Au | PEDOT and *Pd2* Au | PEDOT | Pd samples; **b)** *Pe3* Au | PEDOT and *Pd3* Au | PEDOT | Pd samples; **c)** *Pe4* Au | PEDOT and *Pd4* Au | PEDOT | Pd samples.

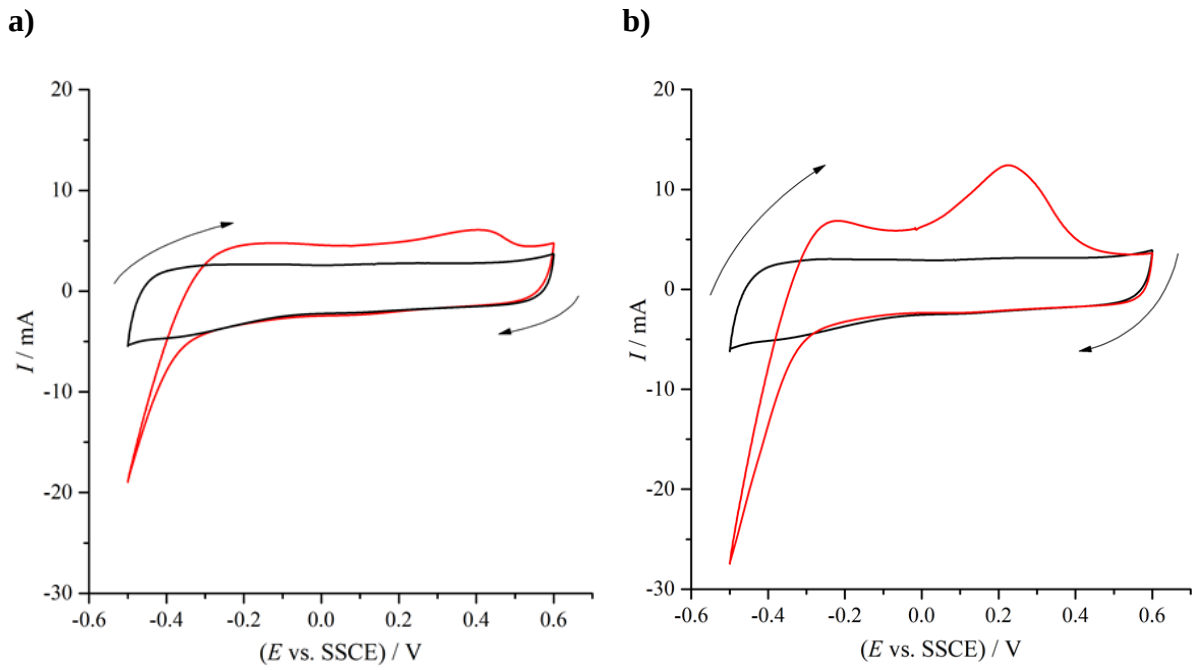

Fig. 10.: Cyclic voltammograms of Au | PEDOT and Au | PEDOT | Pd samples in 0.1 M H_2SO_4. Study of hydrogen evolution. Potential range: (E = -0.5 – +0.6 V) vs. SSCE. Scan rates: 50 mV/s (▬) for Au | PEDOT and 50 mV/s (▬) for Au | PEDOT | Pd. **a)** *Pe3* Au | PEDOT and *Pd3* Au | PEDOT | Pd samples; **b)** *Pe4* Au | PEDOT and *Pd4* Au | PEDOT | Pd samples.

5.2.2. Electrochemical Impedance Spectroscopy

Impedance measurements were carried out on the composite samples as well, thus we are able to compare their high, medium and low frequency behaviour to that of the PEDOT samples. As seen during the impedance analysis of PEDOT, there is no significant potential dependence in the potential range investigated in case of the spectra of PEDOT – palladium composites either. In *Fig. 11.* impedance spectra of the PEDOT – palladium composite *Pd3* are shown.

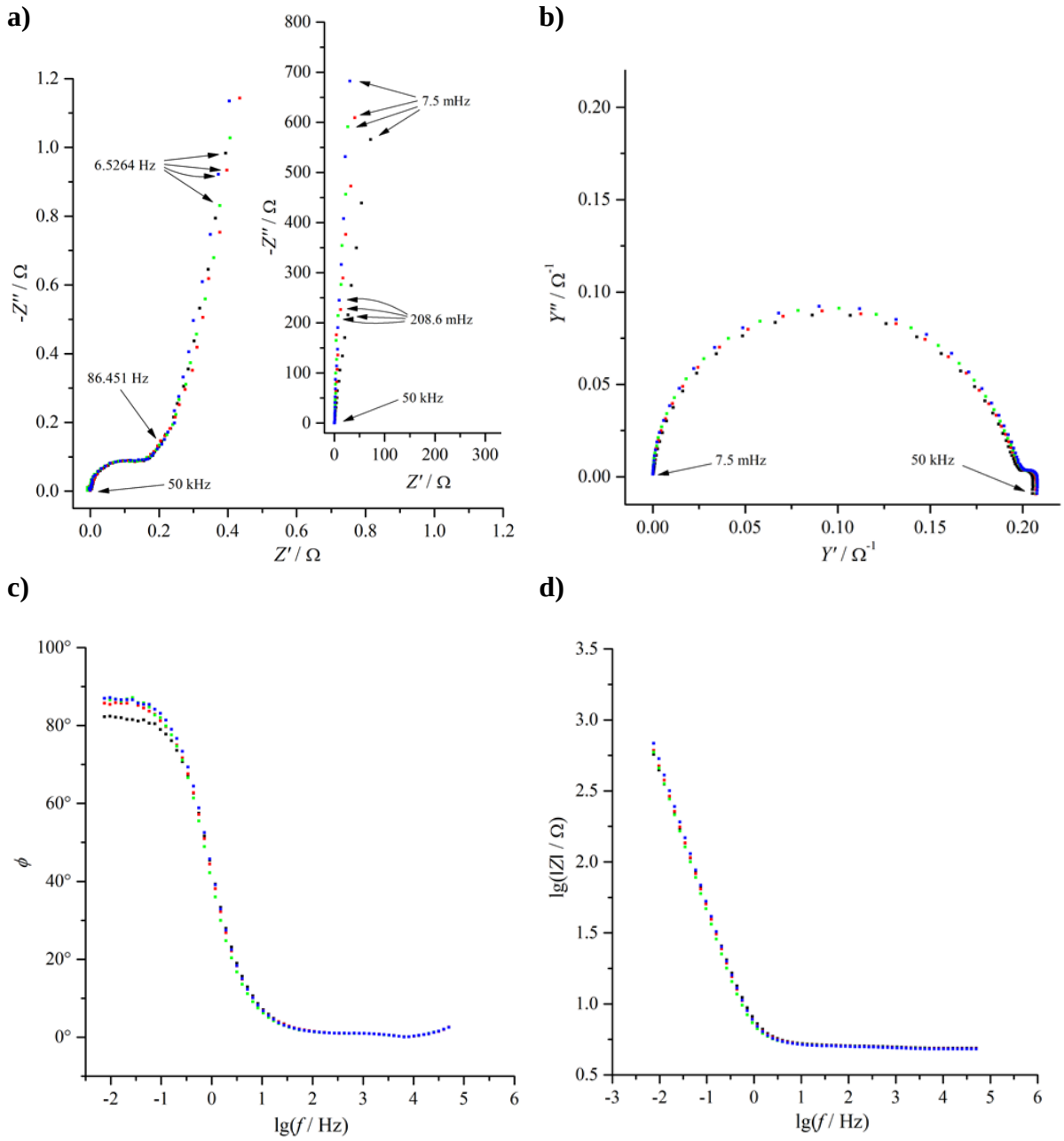

Fig. 11.: Impedance spectra of the Au | PEDOT | Pd sample *Pd3* in 0.1 M H_2SO_4. Electrode potentials: -0.2 (■); 0.0 (■); 0.2 (■); 0.4 (■) V vs. SSCE. **a)** Argand diagrams of the high frequency range and the whole spectra (*Z* ' and *Z* " denoting the real and the imaginary parts of the impedance, respectively); **b)** the imaginary part (*Y* ") of the admittance as a function of the real part (*Y* ') of the admittance; **c)** phase angle as a function of $\lg\tilde{f}$; **d)** $\lg|\tilde{Z}|$ as a function of $\lg\tilde{f}$ ($|\tilde{Z}|$is the modulus of the impedance). ~ signs denote the magnitude of quantities.

The impedance spectra of the PEDOT – palladium composite *Pd3* are fairly similar to those of PEDOT. The Argand diagrams show semicircles at high frequencies, relating to the charge transfer resistance of the composite. At lower frequencies, the curves turn to capacitive saturation. The definite Warburg-like response in the Argand diagram must also be mentioned, however, it seems to be specific only for this composite, as we can see it in the next figures. A comparison of PEDOT and PEDOT – palladium composite samples at two different potentials is displayed in *Fig. 12-14.*

As we can see in the Argand diagrams, each composite has a semicircle at high frequencies, characteristic for the charge transfer at the interfaces. All three Argand-diagrams show capacitive saturation at low frequencies as well, however, the composite samples tend to reach the capacitive saturation earlier. For the composite sample *Pd3* the charge transfer phase doesn't differ significantly from that of the PEDOT sample, contrary to the samples *Pd2* and *Pd4*. The charge transfer resistance shrinked in case of both *Pd2* and *Pd4*. It is also important to notice that the only sample to show a pronounced Warburg-like response is the composite sample *Pd3* (see *Fig.13.*).

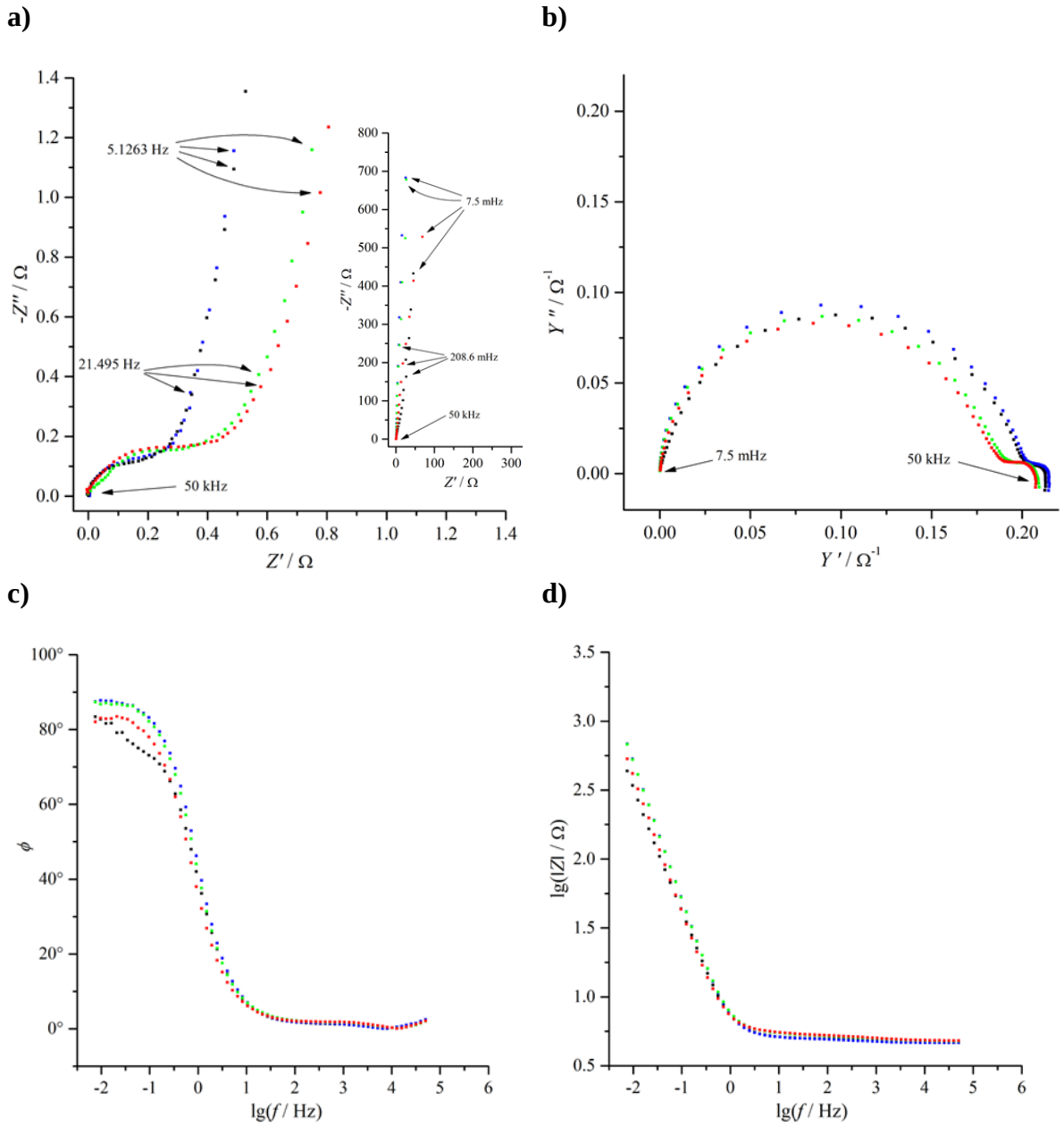

Fig. 12.: Impedance spectra of the *Pe2* Au | PEDOT and *Pd2* Au | PEDOT | Pd samples in 0.1 M H_2SO_4. Electrode potentials: -0.2 (■) and 0.4 (■) V vs. SSCE for Au | PEDOT | Pd sample *Pd2*. and -0.2 (■) and 0.4 (■) V vs. SSCE for Au | PEDOT sample *Pe2*. **a)** Argand diagrams of the high frequency range and the whole spectra (*Z* ' and *Z* '' denoting the real and the imaginary parts of the impedance, respectively); **b)** the imaginary part (*Y* '') of admittance as a function of the real part (*Y* ') of the admittance; **c)** phase angle as a function of $\lg\tilde{f}$; **d)** $\lg|\tilde{Z}|$ as a function of $\lg\tilde{f}$ ($|\tilde{Z}|$is the modulus of the impedance). ~ signs denote the magnitude of quantities.

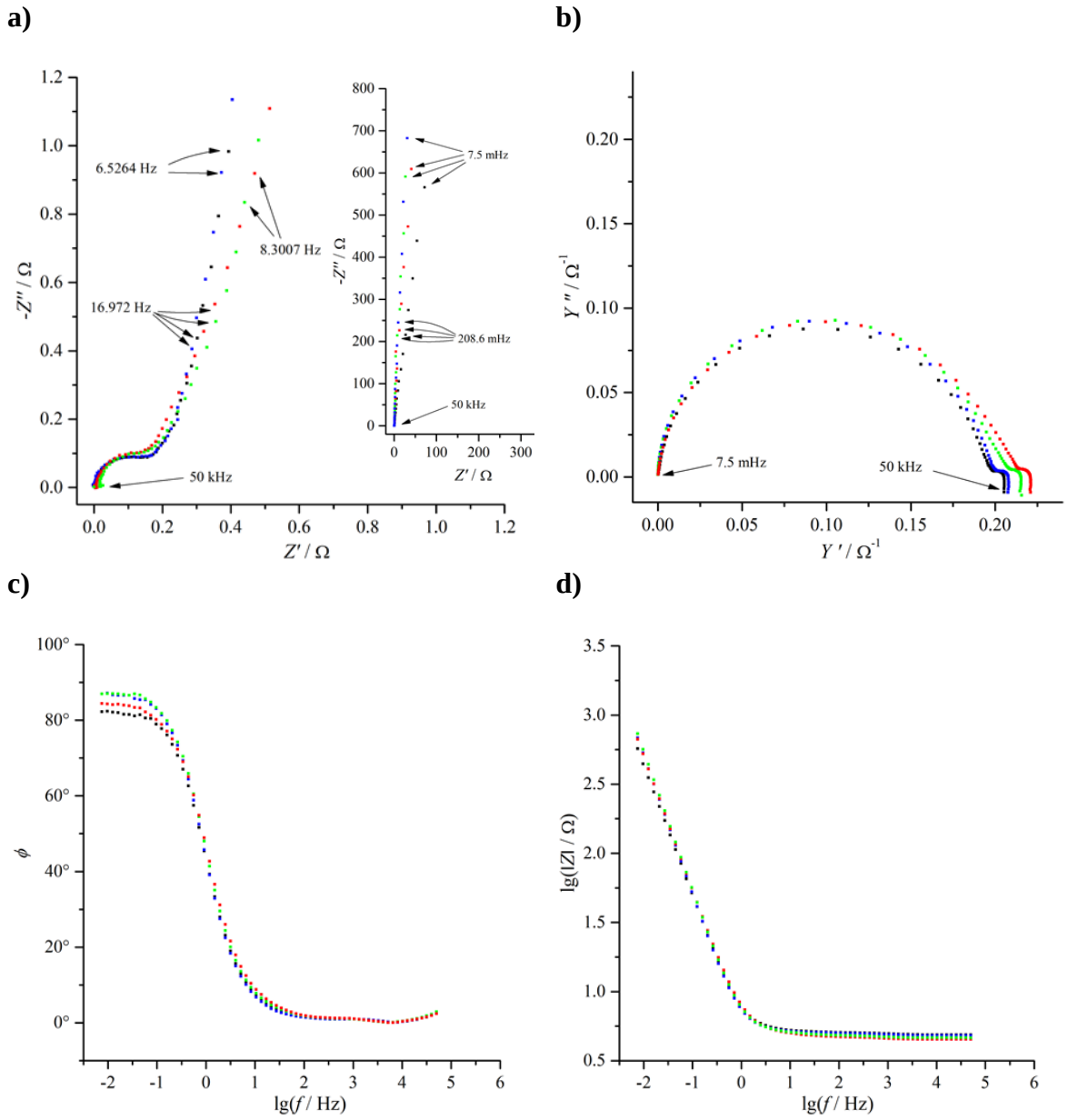

Fig. 13.: Impedance spectra of the *Pe3* Au | PEDOT and *Pd3* Au | PEDOT | Pd samples in 0.1 M H_2SO_4. Electrode potentials: -0.2 (■) and 0.4 (■) V vs. SSCE for Au | PEDOT | Pd sample *Pd3*. and -0.2 (■) and 0.4 (■) V vs. SSCE for Au | PEDOT sample *Pe3*. **a)** Argand diagrams of the high frequency range and the whole spectra (*Z* ' and *Z* '' denoting the real and the imaginary parts of the impedance, respectively); **b)** the imaginary part (*Y* '') of admittance as a function of the real part (*Y* ') of the admittance; **c)** phase angle as a function of $\lg\tilde{f}$; **d)** $\lg|\tilde{Z}|$ as a function of $\lg\tilde{f}$ ($|\tilde{Z}|$is the modulus of the impedance). ~ signs denote the magnitude of quantities.

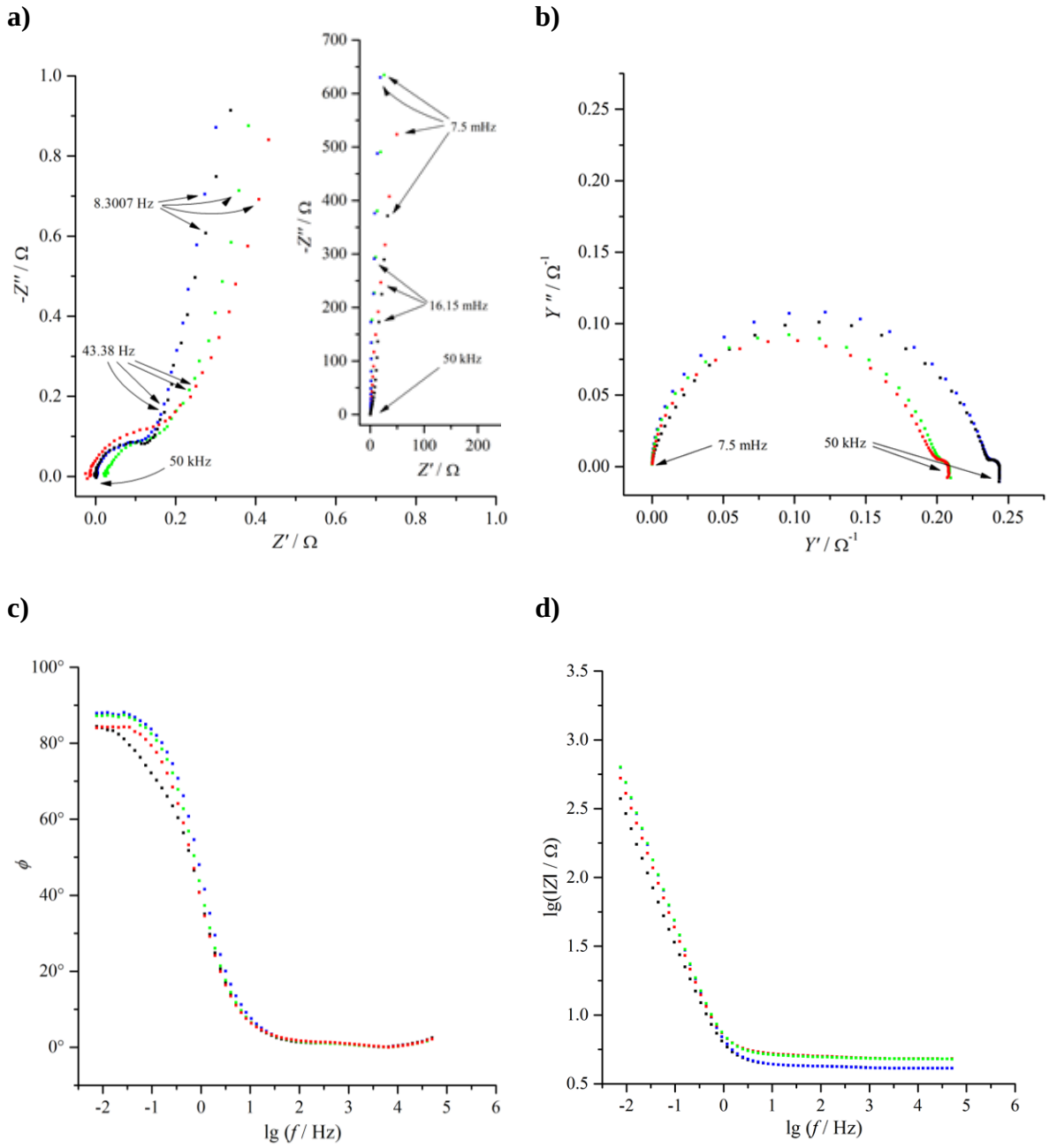

Fig. 14.: Impedance spectra of the *Pe4* Au | PEDOT and *Pd4* Au | PEDOT | Pd samples in 0.1 M H_2SO_4.
Electrode potentials: -0.2 (■) and 0.4 (■) V vs. SSCE for Au | PEDOT | Pd sample *Pd4.* and -0.2 (■) and 0.4 (■) V vs. SSCE for Au | PEDOT sample *Pe4.*
a) Argand diagrams of the high frequency range and the whole spectra (*Z* ' and *Z* '' denoting the real and the imaginary parts of the impedance, respectively); **b)** the imaginary part (*Y* '') of admittance as a function of the real part (*Y* ') of the admittance; **c)** phase angle as a function of $\lg\tilde{f}$; **d)** $\lg|\tilde{Z}|$ as a function of $\lg\tilde{f}$ ($|\tilde{Z}|$is the modulus of the impedance). ~ signs denote the magnitude of quantities.

As it has been mentioned earlier, there are several parameteres which can be estimated by the graphical method. Estimated solution and film resistance (R_s), charge transfer resistance (R_{ct}), Warburg-constant (σ) and small frequency double-layer capacitance (C_{dl})) of the PEDOT – palladium composite samples are shown in *Table 3*. For the graphical and numerical methods used, see the *Appendix*.

Pd1							
E / V	R_s / Ω	R_{ct} / Ω	L / H	f_1 / Hz	f_2 / Hz	σ / Ωs$^{-1/2}$	C_{dl} / mF
0	6.66	0.63	$3.59 \cdot 10^{-7}$	136.17	532.07	9.90	6.76
0.2	6.67	0.62	$3.53 \cdot 10^{-7}$	136.17	532.07	10.34	6.38
0.4	6.68	0.63	$3.51 \cdot 10^{-7}$	136.17	532.07	11.18	5.91
Pd2							
E / V	R_s / Ω	R_{ct} / Ω	L / H	f_1 / Hz	f_2 / Hz	σ / Ωs$^{-1/2}$	C_{dl} / mF
-0.2	4.69	0.26	$6.59 \cdot 10^{-7}$	34.366	170.89	2.97	37.6
0	4.67	0.23	$6.47 \cdot 10^{-7}$	34.366	170.89	3.13	33.9
0.2	4.66	0.24	$6.31 \cdot 10^{-7}$	34.366	170.89	2.64	34.2
0.4	4.65	0.24	$6.51 \cdot 10^{-7}$	34.366	170.89	3.00	31.1
Pd3							
E / V	R_s / Ω	R_{ct} / Ω	L / H	f_1 / Hz	f_2 / Hz	σ / Ωs$^{-1/2}$	C_{dl} / mF
-0.2	4.86	0.19	$6.88 \cdot 10^{-7}$	43.38	337.81	3.28	31.8
0	4.82	0.18	$6.94 \cdot 10^{-7}$	43.38	337.81	3.25	32.6
0.2	4.81	0.18	$6.87 \cdot 10^{-7}$	43.38	337.81	2.67	35.4
0.4	4.81	0.18	$6.87 \cdot 10^{-7}$	43.38	337.81	2.82	31.2
Pd4							
E / V	R_s / Ω	R_{ct} / Ω	L / H	f_1 / Hz	f_2 / Hz	σ / Ωs$^{-1/2}$	C_{dl} / mF
-0.2	4.10	0.19	$5.68 \cdot 10^{-7}$	68.884	214.47	1.74	46.7
0	4.11	0.21	$5.71 \cdot 10^{-7}$	86.45	214.47	1.66	37.3
0.2	4.11	0.18	$5.60 \cdot 10^{-7}$	86.45	214.47	1.57	38.5
0.4	4.10	0.20	$5.73 \cdot 10^{-7}$	68.884	214.47	2.16	33.9

Table 3.: Estimated solution and film resistance (R_s), charge transfer resistance (R_{ct}), inductivity (L), Warburg-constant (σ) and small frequency double-layer capacitance (C_{dl})) for Au | PEDOT | Pd samples *Pd1*, *Pd2*, *Pd3* and *Pd4*. f_1 and f_2 denote the frequency range for the estimation of the Warburg-constant. Measured in 0.1 M H_2SO_4.
Electrode potentials: E = -0.2; 0.0; 0.2 and 0.4 V vs. SSCE.
Surface area: A = 2 cm^2 (*Pd2*, *Pd3*, *Pd4*); A = 1 cm^2 (*Pd1*).

The charge transfer resistance values in *Table 3.* show negligible potential dependence what confirms our earlier conclusions. The frequency range for the determination of the Warburg-constant is the widest and the Warburg-constant is the largest in case of the sample *Pd1,* implying that this composite sample has the most significant diffusional properties. It might be explained by the fact that *Pd1* has lower film thickness than the other samples (see *Table 1.*). Besides, the larger frequency range for the determination of the Warburg-constant suggests a more significant Warburg section in case of the composite sample *Pd3*, (as we could see in *Fig. 14.,* too). The small frequency double layer capacitance values show some fluctuation regarding the potential dependence, however, they tend to be the smallest at the highest potential (E = 0.4 V vs. SSCE). On the other hand, there is no significant difference between the low frequency capacity values of the composite samples with the same surface area and film thickness (*Pd2*, *Pd3*, *Pd4*), but there is a significant difference between the samples of different size and film thickness (*Pd1*).

5.2.3. Scanning Electron Miscroscopy

Distant ETD and vCD images of the surface of a PEDOT – palladium composite can be seen in *Fig.15.*:

a) **b)**

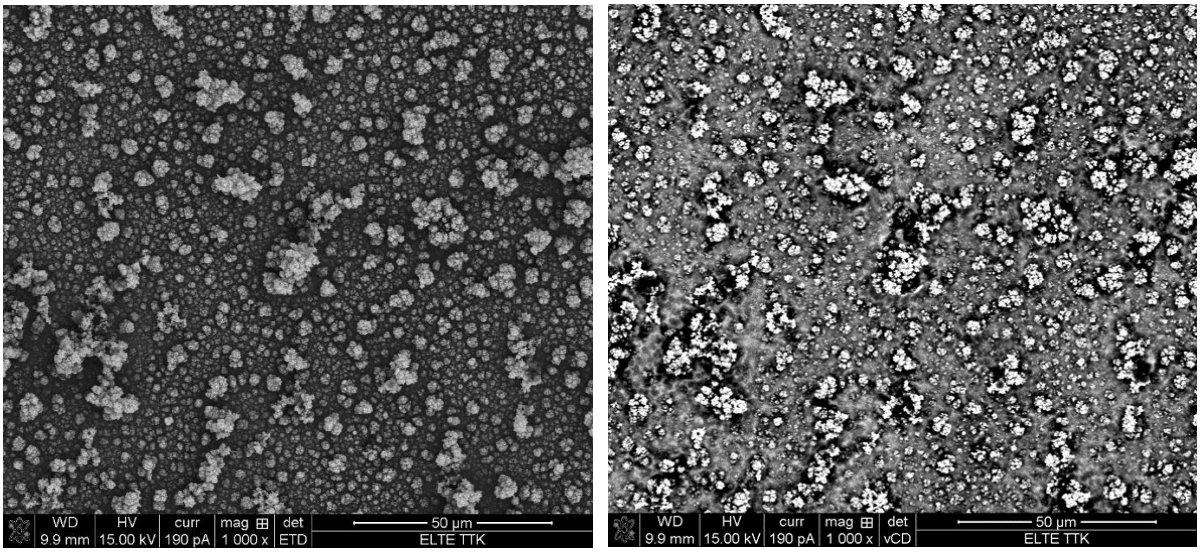

Fig. 15.: SEM images of the *Pd2* Au | PEDOT | Pd sample.
a) Secondary electron image. **b)** Backscattered electron image of the same spot.

PEDOT has a surface with cauliflower-like structures sitting on top of the continuous polymer layer. As we can see in the pictures above, PEDOT – palladium composites have a quite similar surface, the difference is the presence of small palladium crystals, grown preferably on top of the cauliflower structures. The vCD image (*Fig. 15.* **b)**) shows these structures lighter, confirming that the palladium content is higher there than in the continuous polymer layer. (In a vCD image, a spot is shown lighter if more electrons are backscattered from that area and elements with high atomic number backscatter more electrons than those with smaller atomic number.) Palladium crystals can be seen in higher magnification in *Fig. 16.*

a) **b)**

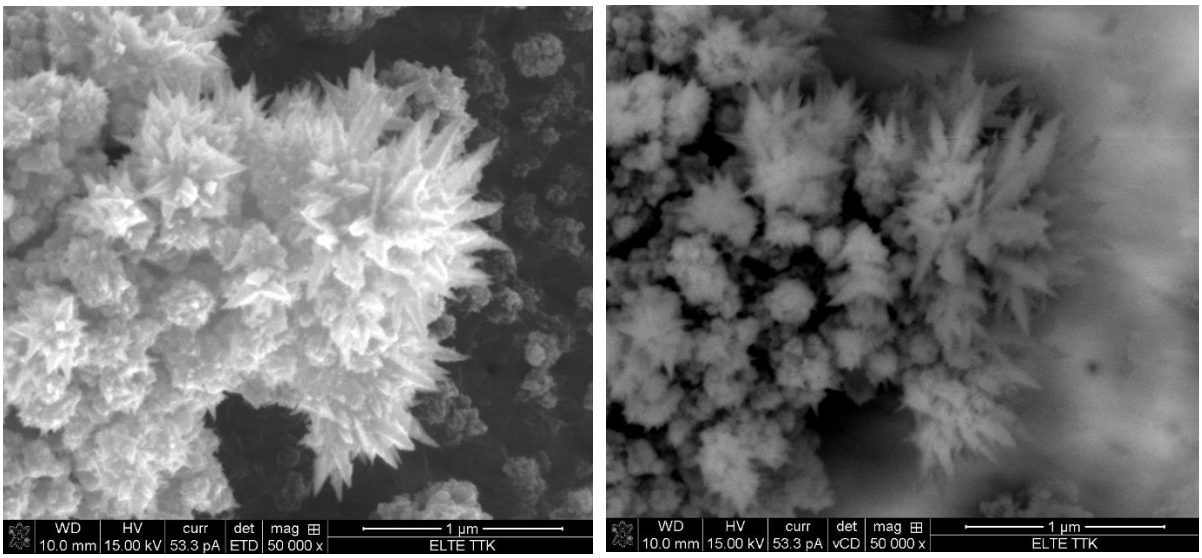

c) **d)**

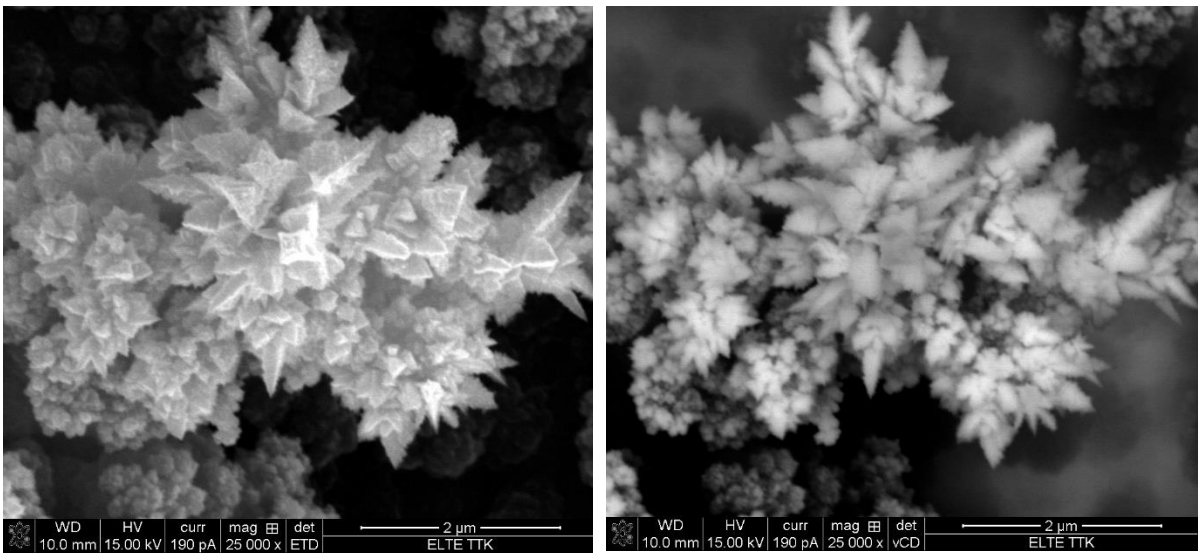

e) **f)**

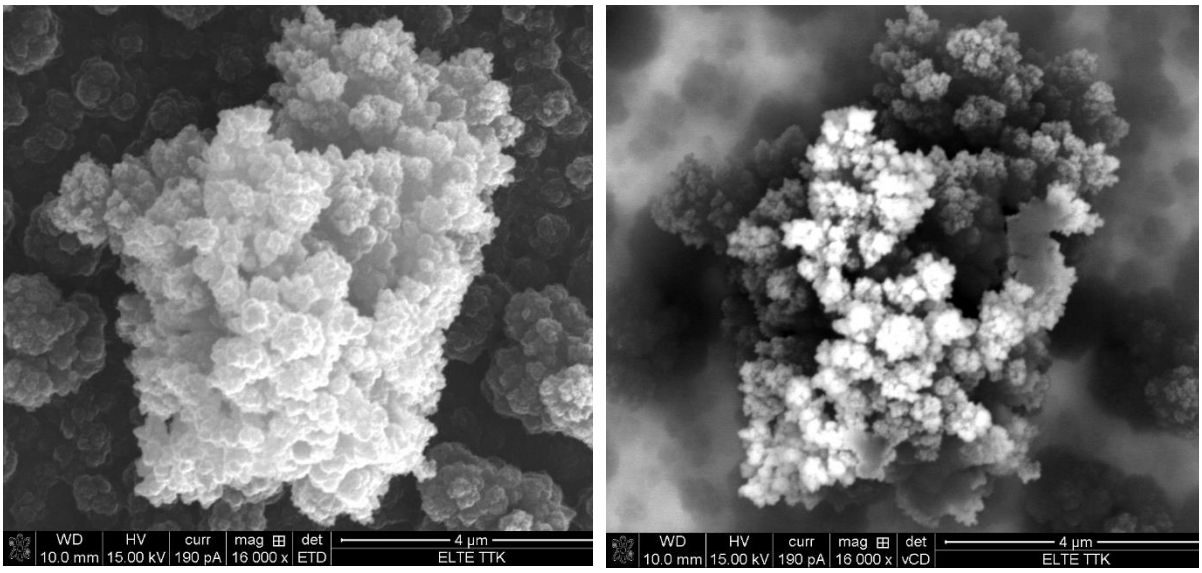

g) **h)**

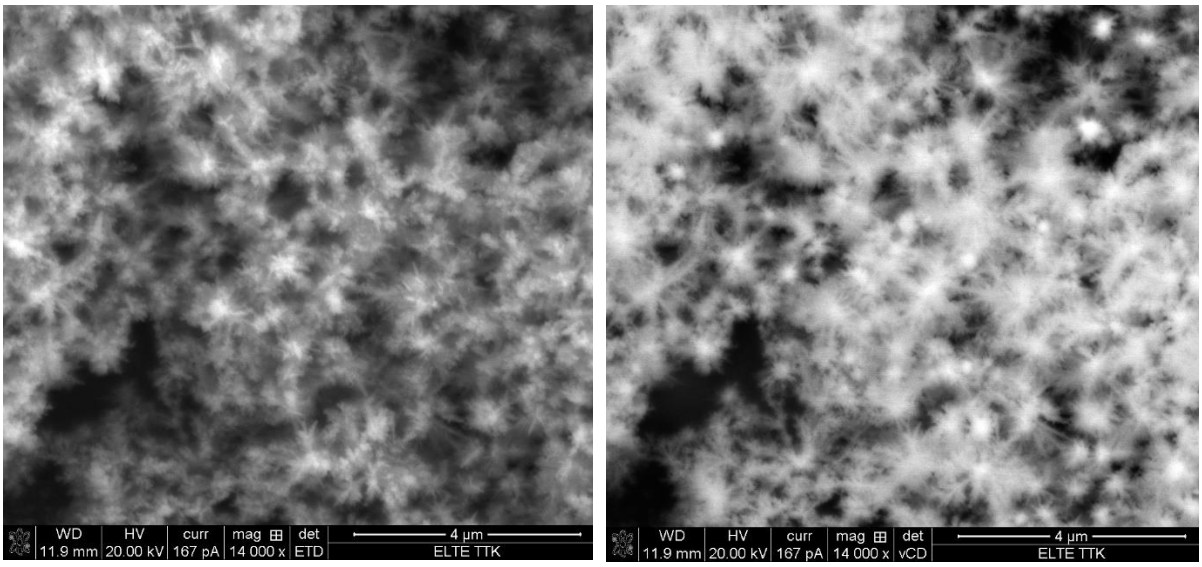

Fig. 16.: SEM images of the Au | PEDOT | Pd samples *Pd1*, *Pd2*, *Pd3* and *Pd4*.
Secondary electron images of **a)** *Pd1***, c)** *Pd2***, e)** *Pd3* and **g)** *Pd4*.
Backscattered electron images of the same spots for **b)** *Pd1***, d)** *Pd2***, f)** *Pd3* and **h)** *Pd4*.

As we can see in *Fig. 16.*, palladium is present in form of small crystals which grow mostly perpendicular to the surface of the "cauliflowers". In case of the composites *Pd1* and *Pd2* (*Fig.16.* **a)** and **c)**), platinum crystals form small spikes, creating a similar, "urchin-like" structure. The size of these spikes is around 0.3-0.8 μm. Small aggregates or flakes indicate the presence of palladium in the composite *Pd3* (*Fig.16.* **e)**), what is confirmed by the vCD image (*Fig.16.* **f)**), too. In case of the composite sample *Pd4*, palladium forms snowflake-like crystals

with an average diameter of ~1μm, while the branches of the snowflakes are in the nanometer range (see *Fig.16.* **g)** and **h)**). These snowflake-like crystals form a three-dimensional, spiderweb-like structure that is rather inhomogeneously distributed on the surface of the composite (see *Fig. 17.* **d)**).

The distribution of palladium is quite inhomogeneous on the surface as we have seen in the SEM images. It would, however, give us a better understanding of the difference of the preparation routes if we could compare the palladium content of the samples. The average palladium content, spots with visible palladium crystals and ditches on the surface are compared in *Table 4.* The measuring spots for the palladium-rich areas and the ditches can be seen in *Fig. 17.*

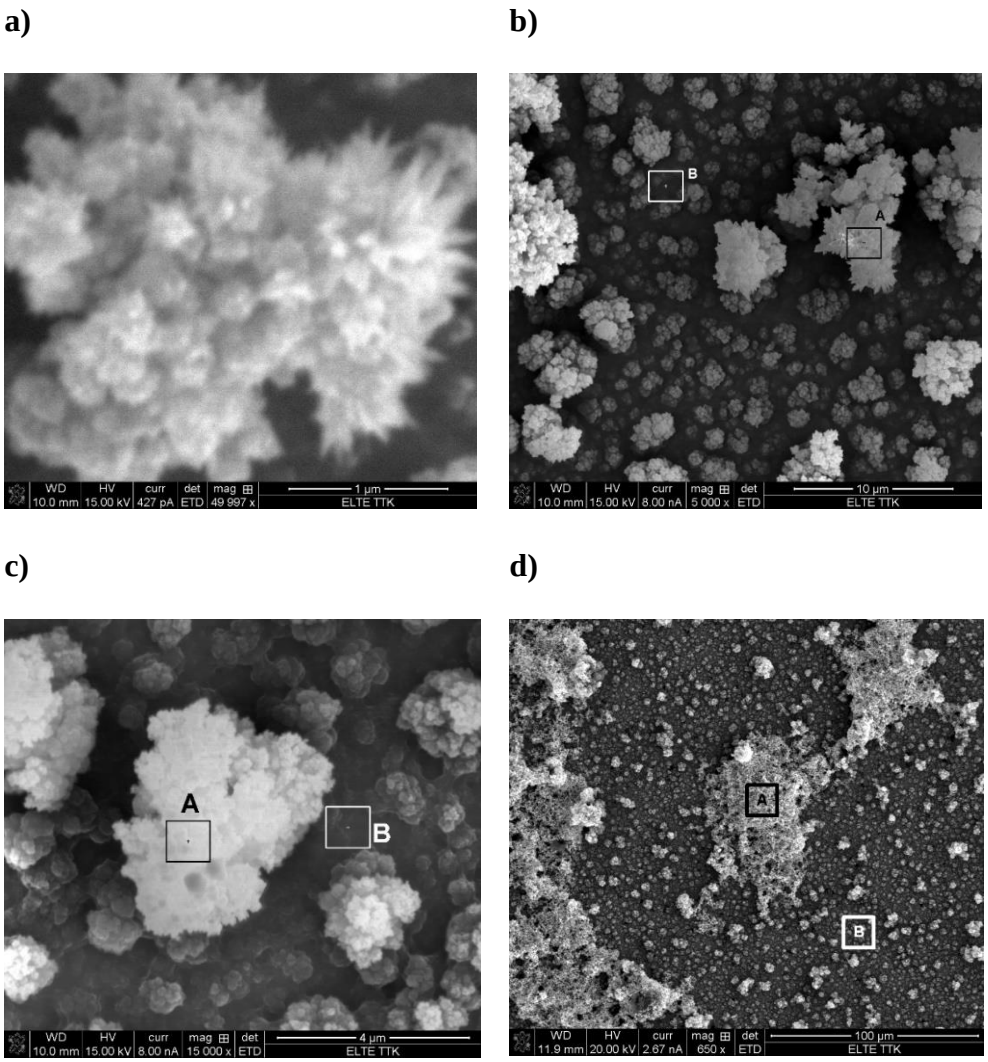

Fig. 17.: Determination of the palladium content of the Au | PEDOT | Pd samples **a)** *Pd1***, b)** *Pd2***, c)** *Pd3* and **d)** *Pd4.*
Spots used for the determination of the palladium content:
a) the whole area of the image (A)**, b)** A**,** B**, c)** A, B and **d)** A, B.

	Pd content (at. %)		
	Average	A	B
Pd1	5.24	16.47	-
Pd2	4.12	28.3	1.59
Pd3	3.15	17.53	1.04
Pd4	4.09	50.80	0.69

Table 4.: Palladium content of the Au | PEDOT | Pd samples.
Average values were measured at distant SEM images.

The values in *Table 4.* suggest that the marked spot of the composite sample *Pd4* has the highest palladium content. Furthermore, palladium content is much lower in the ditches of the composites (B spots) than on the cauliflower structures (A spots), what agrees with our earlier conclusions. The average values correspond to the trend of the A spots, except for the sample *Pd1*. It is the only composite with a thinner (1000 s) polymer film, what explains the higher ratio of the palladium content.

Cross-section images revealed that the film thickness is varied between 0.5 -5 μm for 3600 s PEDOT films (*Pd2*, *Pd3* and *Pd4*), and the penetration of palladium depends significantly on the film thickness. In the upper 1 μm, palladium content is up to 80-100 % of the value on the surface of the samples, while it is only 20-40 % of the surface value in a "deepness" of around 2 μm. A cross-section image with the appropriate measuring spots can be seen in *Fig. 18.*

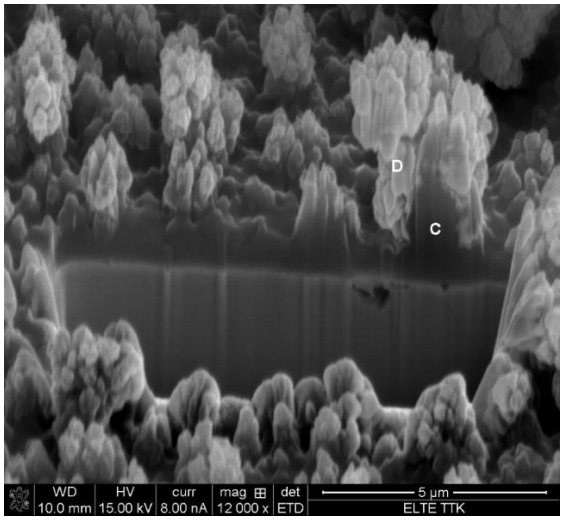

Fig. 18.: Determination of the palladium penetration of the Au | PEDOT | Pd sample *Pd3.*

5.3. Study of PEDOT – platinum composites

5.3.1. Cyclic voltammetry

Cyclic voltammograms recorded on a PEDOT film on a platinum rotating disk electrode can be seen in *Fig. 19.*:

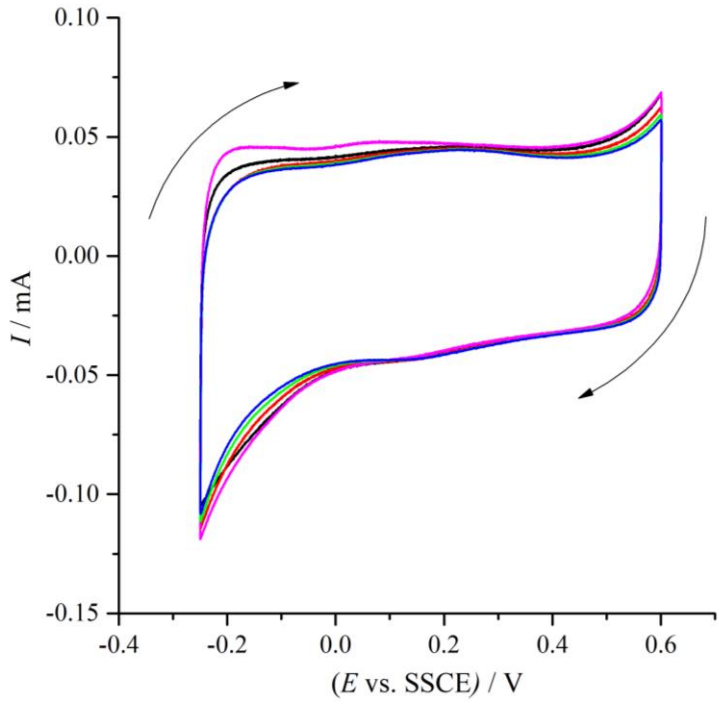

Fig. 19.: Cyclic voltammograms of the Pt | PEDOT sample *Pe5*
in 0.1 M H_2SO_4.
Potential range: (E = -0.25 – +0.6 V) vs. SSCE.
Scan rates: 10 mV/s in argon saturated solution ( ); 10 mV/s in air saturated solution at 0 rpm ( ), 500 rpm ( ), 1000 rpm ( ) and 1500 rpm ( ).

As we can see in *Fig. 19.*, the Pt | PEDOT sample *Pe5* has similar voltammograms in argon saturated and in air saturated solution. Also, there is no rotation rate dependence in the voltammograms recorded in air saturated solution, implying that the Pt | PEDOT sample shows no significant electrocatalytic properties in air.

a) **b)**

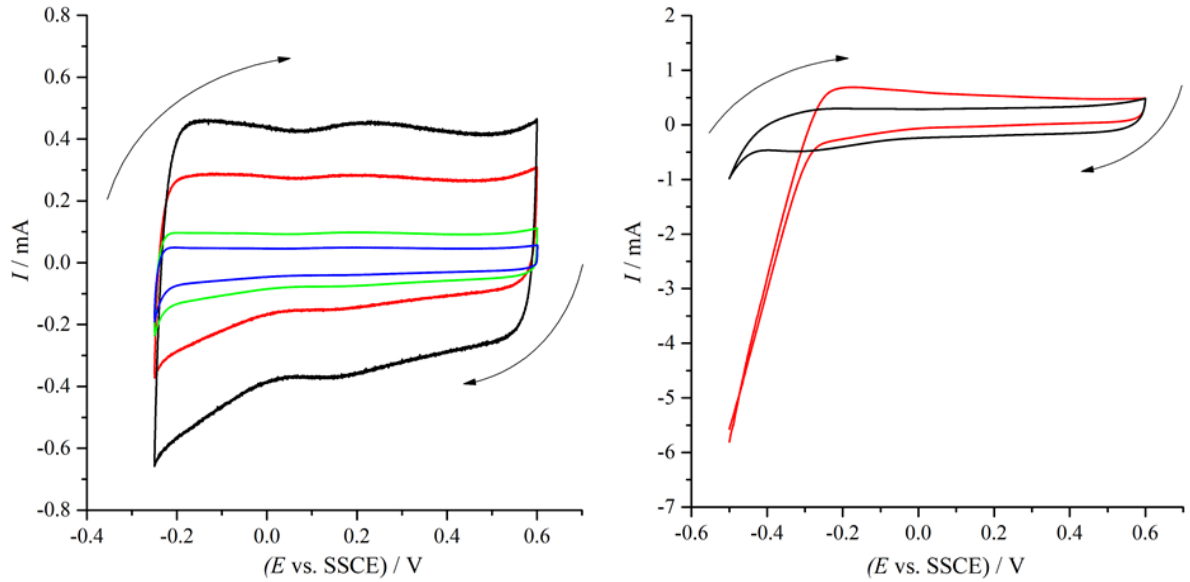

Fig. 20.: Cyclic voltammograms and hydrogen evolution of the Pt | PEDOT sample *Pe5* and Pt | PEDOT | Pt sample *Pt5* in 0.1 M H_2SO_4 saturated with argon.
a) Cyclic voltammograms of the Pt | PEDOT | Pt sample *Pt5*.
Potential range: (*E* = -0.25 – +0.6 V) vs. SSCE.
Scan rates: 100 (▬); 50 (▬); 20 (▬); 10 (▬) mV/s.
b) Hydrogen evolution on the Pt | PEDOT sample *Pe5* and Pt | PEDOT | Pt sample *Pt5*. Potential range: (*E* = -0.5 – +0.6 V) vs. SSCE.
Scan rates: 50 mV/s (▬) for *Pe5* and 50 mV/s (▬) for *Pt5*.

The composite sample *Pt5* has rectangular shaped voltammograms which suggest a capacitive character (see *Fig.20.* **a)**). Cathodic and anodic currrents decrease with the decrease of the scan rate, as expected. *Fig.20.* **b)** shows that the hydrogen reduction reaction increased significantly in case of the composite sample *Pt5*. Hydrogen evolution starts at a more positive potential (~ *E* = -0.3 V vs. SSCE) and the peak current at the negative end of the potential range is approximately six times larger than for the PEDOT sample.

Cyclic voltammograms were also recorded in air saturated solution to study the electrocatalytic properties of the composite sample (*Fig.21.*).

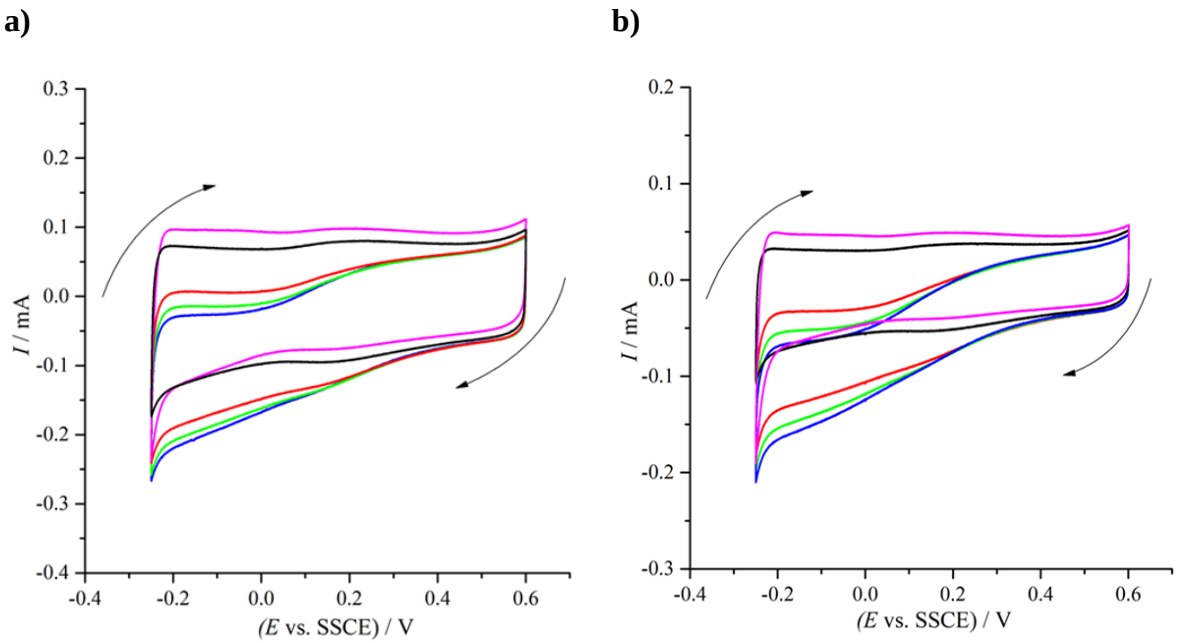

Fig. 21.: Study of the electrocatalytic properties of the Pt | PEDOT | Pt sample *Pt5*.
Recorded in 0.1 M H_2SO_4 saturated with air.
Potential range: (E = -0.25 – +0.6 V) vs. SSCE.
a) Scan rates: 20 mV/s in argon atmosphere ( ); 20 mV/s in air atmosphere at 0 rpm ( ), 500 rpm ( ), 1000 rpm ( ) and 1500 rpm ( ).
b) Scan rates: 10 mV/s in argon atmosphere ( ); 10 mV/s in air atmosphere at 0 rpm ( ), 500 rpm ( ), 1000 rpm ( ) and 1500 rpm ( ).

As we can see in *Fig. 21.*, cyclic voltammograms recorded in air saturated solution differ to a great extent from those recorded using argon atmosphere. Cycles slide down towards the negative end of the potential range, what implies that another process with significant reductive current is taking place in that potential range. The sliding down of the voltammograms is even more significant at a lower scan rate (*Fig. 21.* **b)**) suggesting a sluggish, diffusional character for the electrocatalysed reaction taking place. This assumption is confirmed by the unambiguous rotation rate dependence of the cycles,too. *Fig. 22.* shows that the Levich equation is fulfilled in the solution saturated with air, i.e. diffusion-control is present in case of the catalysed reaction taking place in this potential range (see the equation (7)). (For the determination of the limiting currents, see the *Appendix*).

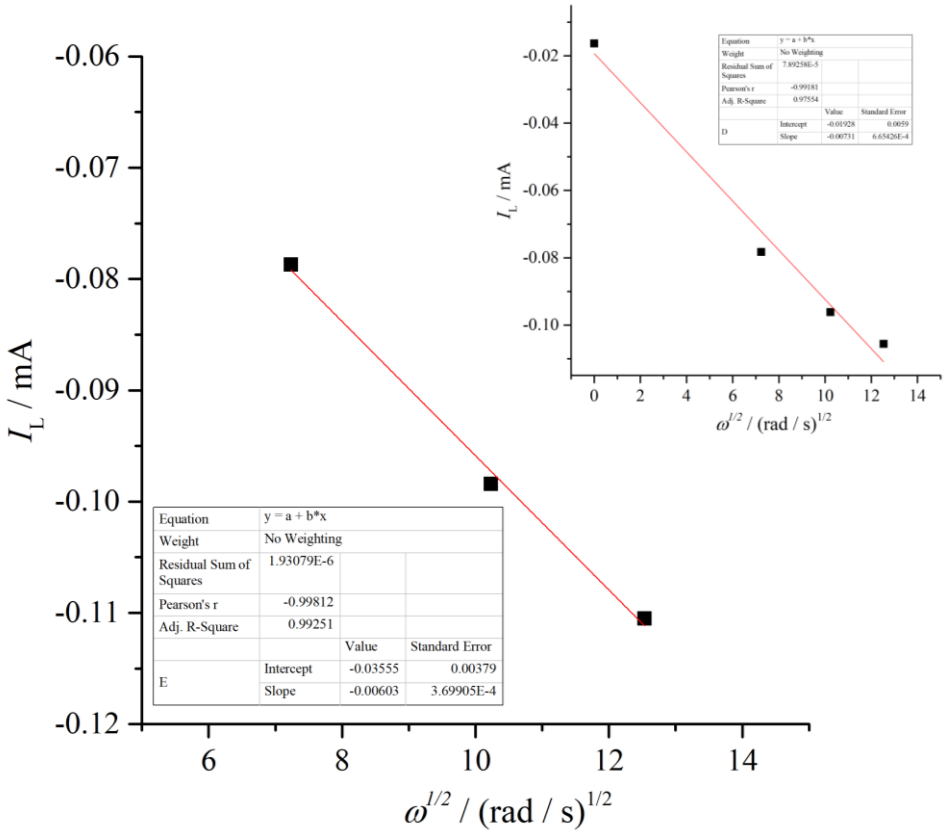

Fig. 22.: Levich plot recorded on the Pt | PEDOT | Pt sample *Pt5*.
Limiting current (I_L) as a function of the square root of the angular rotation rate ($\omega^{1/2}$).
Recorded in 0.1 M H_2SO_4 saturated with air.
Potential range: (E = -0.25 – +0.6 V) vs. SSCE.
Scan rate: 10 mV/s.

5.3.2. Electrochemical Impedance Spectroscopy

The rotation rate dependence of the impedance spectra of the samples *Pe5* and *Pt5* can be seen in *Fig. 23.*

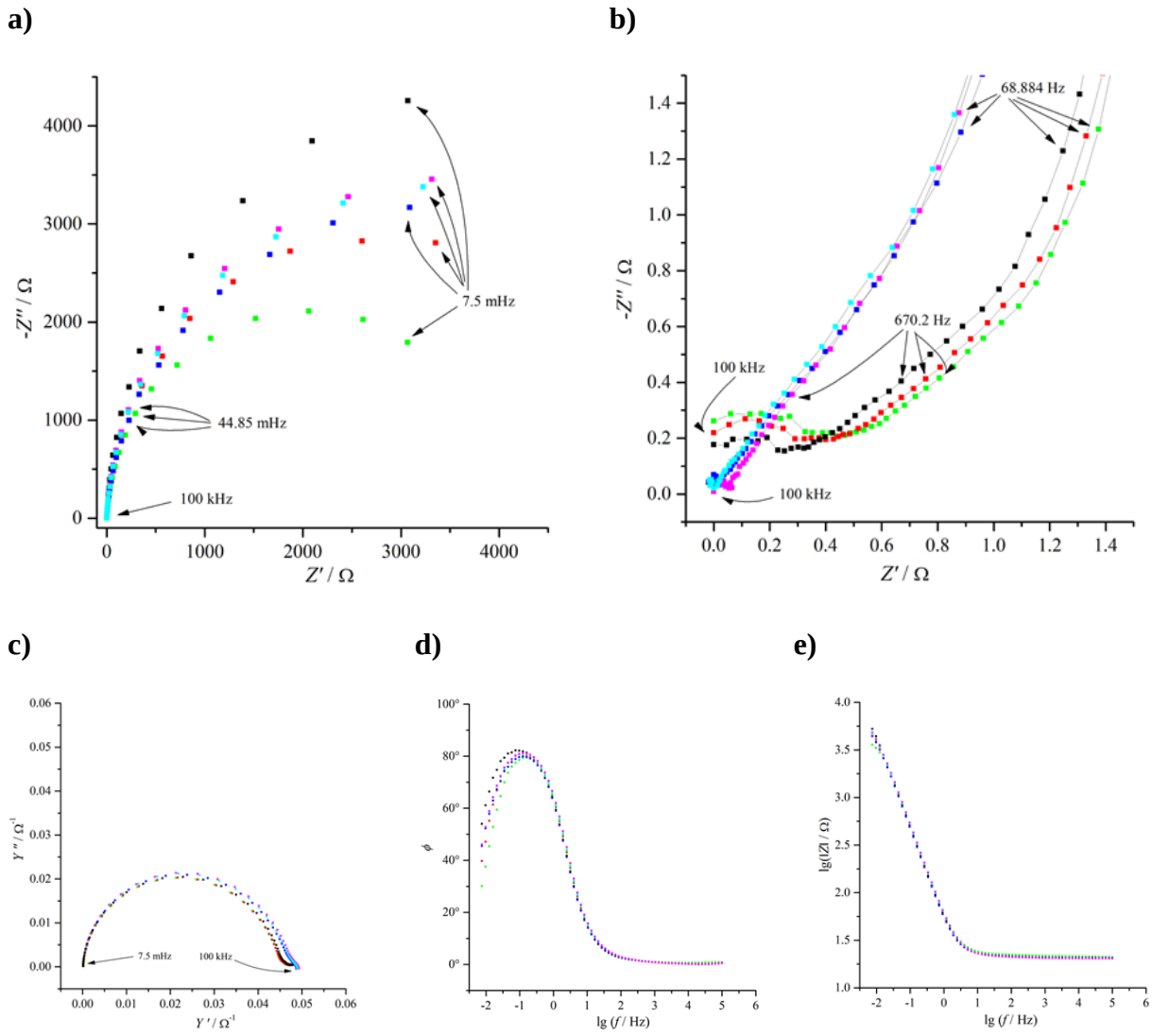

Fig. 23.: Rotation rate dependence of the impedance spectra of *Pe5* Pt | PEDOT and *Pt5* Pt | PEDOT | Pt samples.
Recorded in 0.1 M H_2SO_4 saturated with air.
Electrode potential: (E = -0.2 V) vs. SSCE.
Rotation rates: 500 rpm (■), 1000 rpm (■) and 1500 rpm (■) for Pt | PEDOT | Pt sample *Pt5* and 500 rpm (■), 1000 rpm (■) and 1500 rpm (■) for Pt | PEDOT sample *Pe5.*
a) Argand diagram of the whole spectra (Z ' and Z '' denoting the real and the imaginary parts of the impedance, respectively); **b)** Argand diagram of the high frequency range. (Lines in the graph are not fits, they serve purely the easier visualisation); **c)** the imaginary part (Y '') of the admittance as a function of the real part (Y ') of the admittance; **d)** phase angle as a function of $\lg\tilde{f}$; **e)** $\lg|\tilde{Z}|$ as a function of $\lg\tilde{f}$ ($|\tilde{Z}|$is the modulus of the impedance).
~ signs denote the magnitude of quantities.

The impedance spectra of the composite sample *Pt5* show unambiguous rotation rate dependence, contrary to the PEDOT sample *Pe5*. *Fig.23.* **a)** shows that in case of the sample *Pt5* the low frequency region of the imaginary part of the impedance decreases significantly with higher rotation rates, referring to the presence of a sluggish reaction taking place. Besides, the charge transfer resistance of the composite sample *Pt5* increases with higher rotation rates as we can see in the high frequency region of the impedance spectra (*Fig.23.* **b**). The PEDOT sample *Pe5* shows no significant rotation rate dependence, however, both samples show a distinct Warburg-section as we can see in *Fig.23.* **b)**.

Fig.24. suggests that the impedance spectra of the sample *Pe5* show no significant potential dependence in air saturated solution, contrary to those of the composite sample *Pt5*. The charge transfer resistance of the composite sample increases to a great extent at more negative potentials (see the green, red and black dots in *Fig.24.* **b)**). Besides, the impedance spectra of the sample *Pt5* bend down considerably in the low frequency region, suggesting the presence of another process taking place at low frequencies (*Fig.24.* **a)**). The Bode-plot (*Fig.24.* **d)**) shows a significant difference between the spectra of the *Pe5* and *Pt5* samples. In case of the sample *Pe5*, an incline in the low frequency region of the spectra can be observed only at the lowest potential (E = -0.2 V vs. SSCE, blue dots in *Fig.24.* **d)**), while the low frequency region of the spectra of *Pt5* slide down to a great extent, suggesting the presence of a catalysed reaction at each potential.

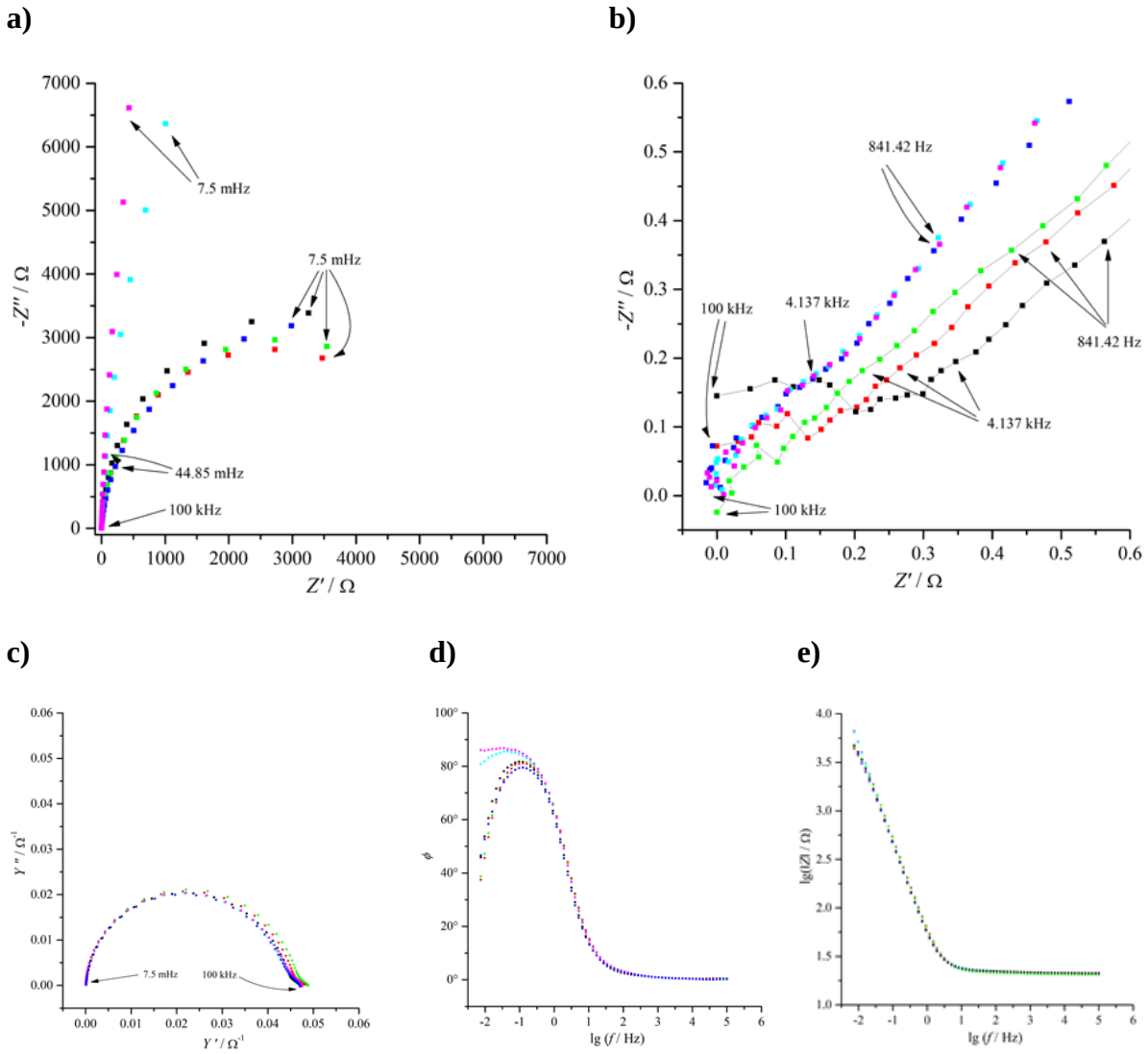

Fig. 24.: Potential dependence of the impedance spectra of *Pe5* Pt | PEDOT and *Pt5* Pt | PEDOT | Pt samples.
Recorded in 0.1 M H_2SO_4 saturated with air.
Rotation rate: 1000 rpm.
Electrode potentials: -0.2 (■), -0.1 (■) and 0.0 (■) V vs. SSCE
for Pt | PEDOT | Pt sample *Pt5* and -0.2 (■), -0.1 (■) and 0.0 (■) V vs. SSCE
for Pt | PEDOT sample *Pe5*.
a) Argand diagram of the whole spectra (*Z* ' and *Z* " denoting the real and the imaginary parts of the impedance, respectively); **b)** Argand diagram of the high frequency range. (Lines in the graph are not fits, they serve purely the easier visualisation); **c)** the imaginary part (*Y* ") of the admittance as a function of the real part (*Y* ') of the admittance; **d)** phase angle as a function of $\lg\tilde{f}$; **e)** $\lg|\tilde{Z}|$ as a function of $\lg\tilde{f}$ ($|\tilde{Z}|$is the modulus of the impedance).
~ signs denote the magnitude of quantities.

6. Conclusions

We have seen that the preparation methods based on the literature proved to be effective and resulted in varied PEDOT – palladium composites. Cyclic voltammetry, electrochemical impedance spectroscopy and scanning electron microscopy studies were carried out to characterize the electochemical properties and the morphology of the obtained composites. The cyclic voltammograms of the composite samples showed no significant differences in the potential range of E = (-0.25 – + 0.6) V vs. SSCE, as we can see in *Fig.25.* **a)**. The capacitive currents of the sample *Pd1* are smaller than those of the other samples what can be explained by the lower film thickness of the sample (1000 s deposition time, see *Table 1.*). We have also seen that significant hydrogen evolution takes place on the surface of the composites at more negative potentials (see *Fig.25.* **b)**). The magnitude of the hydrogen reduction peaks are quite similar in case of the samples *Pd2* and *Pd4* what agrees with the approximately equal average palladium content according to the EDX measurements.

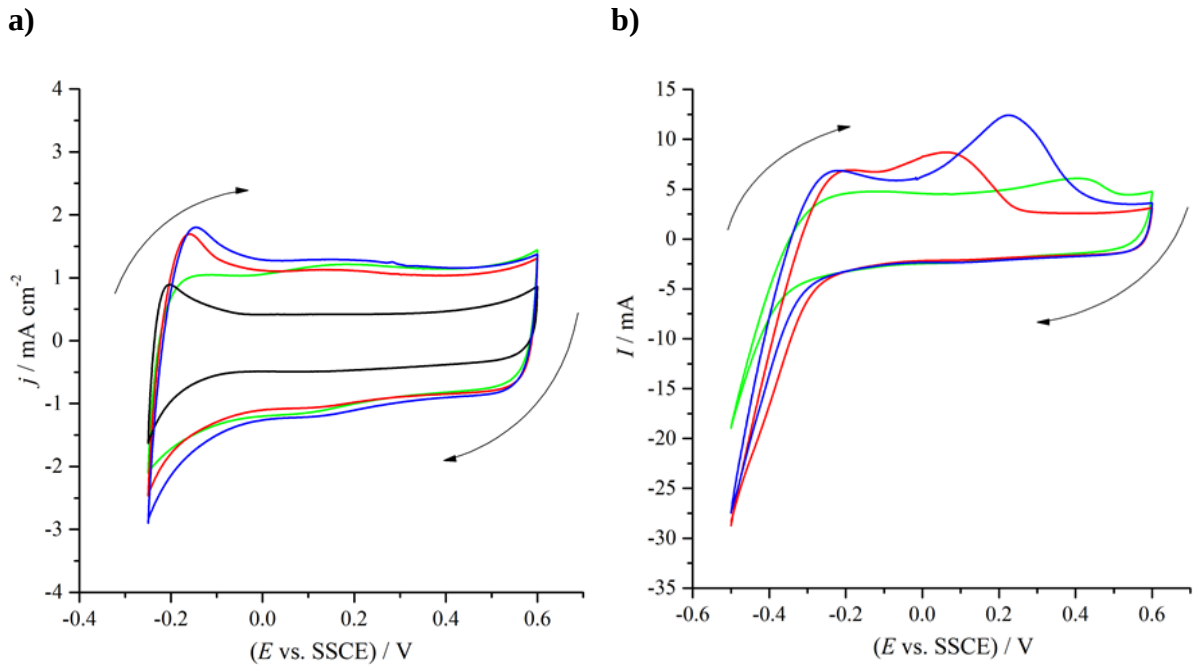

Fig. 25.: Cyclic voltammograms and hydrogen evolution of Au | PEDOT | Pd samples in 0.1 M H_2SO_4.
a) Cyclic voltammograms of Au | PEDOT | Pd samples.
Potential range: (E = -0.25 – +0.6 V) vs. SSCE.
Scan rates: 50 mV/s for *Pd1* ( ); *Pd2* ( ); *Pd3* ( ) and *Pd4* ( ).
b) Hydrogen evolution on Au | PEDOT | Pd samples.
Potential range: (E = -0.5 – +0.6 V) vs. SSCE.
Scan rates: 50 mV/s for *Pd2* ( ); *Pd3* ( ) and *Pd4* ( ).

The electrochemical impedance spectroscopy measurements showed that there is no significant potential dependence in the impedance spectra of the PEDOT – palladium composites. The charge transfer resistance of the samples *Pd2* and *Pd4* shrinked compared to that of PEDOT. The small frequency double layer capacity values were of similar magnitude for each composite of the same film thickness and surface area. The sample *Pd3* showed a definite Warburg-section which may be related to the structure of the composite caused by the electroless preparation. The Warburg constant was, however, the largest in case of the sample *Pd1*, what might be expained by the lower film thickness and thus better diffusion within the film.

The scanning electron microscopy studies revealed that the deposited palladium crystals are distributed rather inhomogeneously on the surface of the composites. The samples of the same preparation technnique (*Pd1* and *Pd2*) had a similar, urchin-like structure where palladium crystals formed spikes growing preferably on top of the cauliflower-like structures of the polymer film. The electroless palladium deposition resulted in small aggregates and flakes of palladium in case of the sample *Pd3*, whereas the SEM images of the sample *Pd4* showed snowflake-like palladium crystals which formed spiderweb-like structures. The finer structure of the snowflake-like palladium crystals might be explained by the larger overpotential applied during the reduction and the immersion. While the local palladium content was far the highest within these spiderweb-like structures, the average palladium content of the composites do not differ considerably.

A Pt | PEDOT | Pt composite was also prepared on a platinum rotating disk electrode and studied both in argon and air saturated solution. The PEDOT film (sample *Pe5*) showed similar voltammograms in the solution saturated with argon and with air, no rotation rate dependence was observed during the study of the sample. On the contrary, the Pt | PEDOT | Pt composite sample showed significant rotation rate dependence in air saturated solution which became more pronounced at lower scan rates. The rotation rate dependence fulfilled the Levich-equation (see *Fig.22.*), what confirmed the assumption of the diffusion-controlled character of the reaction taking place on the composite sample. The impedance analysis also confirmed the considerable rotation rate dependence in case of the composite sample *Pt5*. On the contrary, no significant rotation rate dependence could be observed in case of the PEDOT sample *Pe5*. On the other hand, the impedance spectra recorded in air saturated solution also showed unambiguous potential dependence in case of the composite sample.

A future objective based on this thesis could be the study of the catalytic properties of the obtained Au | PEDOT | Pd composites in varied solutions. Besides, the development of dedicated composite systems for specific applications could be highly beneficial. On the other hand, the further study of the electrocatalytic properties of Pt | PEDOT | Pt composite systems in oxygen saturated solution is inevitable to unambiguously prove the presence of the oxygen reduction reaction.

Thesis summary

Preparation and study of composites based on poly(3,4-ethylenedioxythiophene)

Levente Juhász, MSc student in Materials Science

Department of Physical Chemistry, Institute of Chemistry, Eötvös Loránd University, Budapest

Supervisors: **Dr. Győző Láng,** professor
Department of Physical Chemistry, Eötvös Loránd University
Dr. Mária Ujvári, assistant professor
Department of Physical Chemistry, Eötvös Loránd University

During my Master's studies, I joined the Laboratory of Electrochemistry and Electroanalytical Chemistry at the Eötvös Loránd University where I engaged in the research on composites based on poly(3,4-ethylenedioxythiophene), i.e PEDOT. PEDOT is a widely used conducting polymer owing to its advantageous properties, however, it is often used in the form of composites for dedicated applications.

PEDOT – palladium and PEDOT – platinum composites stand in the limelight of science due to their special electrocatalytic properties, little information is found in papers, however, on the electrochemical study of "pure" composite systems without additives. On the other hand, the disambiguation of the effects of the preparation conditions on the electrochemical properties and morphology of PEDOT – palladium composites would be highly beneficial.

Four different PEDOT – palladium composite samples were prepared by the immersion of PEDOT films into 0.005 M $PdCl_2$ - 0.1 M H_2SO_4 solution, using different preparation methods with varied film reduction and immersion parameters. The obtained composite systems were studied by cyclic voltammetry and electrochemical impedance spectroscopy in 0.1 M aqueous sulphuric acid solution. The morphology and the palladium content of the composites were studied by scanning electron microscopy.

The cyclic voltammograms of the PEDOT – palladium composite samples showed little difference in the potential range of E = (-0.25 – +0.6) V vs. SSCE, compared to those of PEDOT. On the other hand, significant hydrogen reduction peaks could be observed at more negative potentials in case of the composite samples. The impedance spectra of the composite samples showed no significant potential dependence, besides, the small frequency double layer capacity values were similar in case of the composites of the same surface area and film thickness. One of the composite samples showed a distinct Warburg section at medium frequencies what may be related to the structure caused by the electroless composite preparation method. Scanning electron microscopy measurements showed that the palladium crystals formed spikes, aggregates and snowflakes on top of the PEDOT film, depending on the preparation method used. The distribution of palladium was considerably inhomogeneous, while the average palladium content of the samples did not differ to a large extent.

A PEDOT – platinum composite on a platinum rotating disk electrode was also prepared and studied in this thesis. Cyclic voltammetry and electrochemical impedance spectroscopy measurements were carried out both in argon and air saturated 0.1 M sulphuric acid to study the electrocatalytic properties of the composite. The cyclic voltammograms of the PEDOT – platinum composite sample showed significant rotation rate dependence in air saturated solution, contrary to PEDOT. Furthermore, the Levich equation was fulfilled in case of the composite sample, suggesting the presence of a sluggish, diffusion-controlled reaction in air saturated solution. The impedance spectra of the composite sample confirmed the rotation rate dependence, in contrast to those of PEDOT.

Szakdolgozat összefoglaló

Poli(3,4-etiléndioxitiofén)-alapú kompozitok előállítása és vizsgálata

Juhász Levente, anyagtudomány mesterszakos hallgató

ELTE TTK Kémia Intézet, Fizikai Kémia Tanszék

Témavezetők: **Dr. Láng Győző,** egyetemi tanár
ELTE TTK Kémia Intézet
Dr. Ujvári Mária, egyetemi adjunktus
ELTE TTK Kémia Intézet

Anyagtudomány mesterszakos tanulmányaim során az ELTE Elektrokémiai és Elektroanalitikai Laboratóriumának munkájába kapcsolódtam be, ahol poli(3,4-etiléndioxitiofén)-, azaz PEDOT-alapú vezető kompozitok előállításával foglalkoztam. Számos előnyös tulajdonságának köszönhetően a PEDOT széles körben használt elektromosan vezető polimer, szintén gyakoriak azonban a PEDOT kompozit alapú alkalmazásai is.

A PEDOT-alapú rendszerek közt a PEDOT – palládium és PEDOT – platina alapú kompozitok főként különleges elektrokatalitikus tulajdonságaik miatt keltették fel a tudomány érdeklődését, kevés információ áll azonban rendelkezésre "tiszta", adalékanyagoktól mentes kompozitok elektrokémiai vizsgálatáról. Másfelől szintén nem teljes mértékben tisztázott az irodalomban említett különböző kompozit előállítási módszerek és a kompozitok elektrokémiai tulajdonságai, illetve szerkezete közötti kapcsolat, így ezek mélyebb ismerete a jövőben a kompozitok hatékonyabb tervezését tenné lehetővé.

Munkám során négy különböző PEDOT – palládium kompozitot állítottam elő PEDOT filmek 0,005 M $PdCl_2$ – 0,1 M H_2SO_4-oldatba történő bemerítésével. A bemerítés előtt a PEDOT filmeket különböző potenciálokon redukáltam, illetve a bemerítés során a filmeket különböző potenciálokon tartottam. Az így előállított kompozitokat ciklikus voltammetriával, elektrokémiai impedancia spektroszkópiával és pásztázó elektronmikroszkóppal vizsgáltam.

Az előállított kompozitok ciklikus voltammogramjai egymáshoz igen hasonlóak voltak az E = (-0,25 – +0,6) V vs. SSCE potenciáltartományban, kapacitív jelleget mutattak a PEDOT filmek ciklikus voltammogramjaihoz hasonlóan. Negatívabb potenciálokon azonban jelentős mértékű hidrogénfejlődés volt tapasztalható a kompozit minták esetén, ellentétben a PEDOT filmekkel. A kompozit minták impedancia spektrumai a PEDOT-hoz hasonlóan csupán kismértékű potenciálfüggést mutattak, emellett a kompozitok kisfrekvenciás kettősréteg kapacitás értékei is többnyire hasonló nagyságúak voltak azonos filmvastagság és felület esetén. Az egyik kompozit minta Argand-diagramján határozott Warburg-szakasz volt megfigyelhető közepes frekvenciáknál, mely a potenciál alkalmazása nélküli bemártással történő előállítás során kialakult szerkezettel lehet összefüggésben. A pásztázó elektronmikroszkópos felvételek szerint az előállítási módszertől függően a palládium tüske, lemez és hópehely alakú kristályokat képez a PEDOT réteg karfiol-szerű képződményein. A pásztázó elektronmikroszkópon végzett energiadiszperzív röntgen mikroanalízis alapján a kompozit minták felületén igen inhomogén a palládium eloszlása, a kompozit minták átlagos palládium-tartalma azonban közel azonos.

Jelen dolgozat második felében egy PEDOT – platina kompozitot állítottam elő platina forgó korongelektródon. A Pt | PEDOT | Pt kompozit elektrokatalitikus tulajdonságait ciklikus voltammetriával és elektrokémiai impedancia spektroszkópiával vizsgáltam argonnal illetve levegővel telített 0,1 M koncentrációjú kénsavban. A PEDOT – platina kompozit ciklikus voltammogramjai és impedancia spektrumai egyértelmű fordulatszámfüggést mutattak levegővel telített oldatban, míg a PEDOT minta esetén nem volt észrevehető fordulatszámfüggés. A kompozit mintán mért fordulatszámfüggés teljesítette a Levich-egyenletet, megerősítve a feltételezést, hogy a levegővel telített oldatban egy lassú, diffúzió-kontrollált reakció játszódik le a kompozit mintán.

Appendix

A1 Electrochemical cleaning by cyclic voltammetry

The electrochemical cleaning of a metal electrode is carried out as cyclic voltammetry, but in a wider potential range where the metal electrode itself takes part in a redox reaction. This technique is suitable for removing contaminations of the surface of the electrode whilst smoothing the surface of the electrode as well. Cleaning voltammograms of a gold and a platinum electrode can be seen in *Fig.A1*.

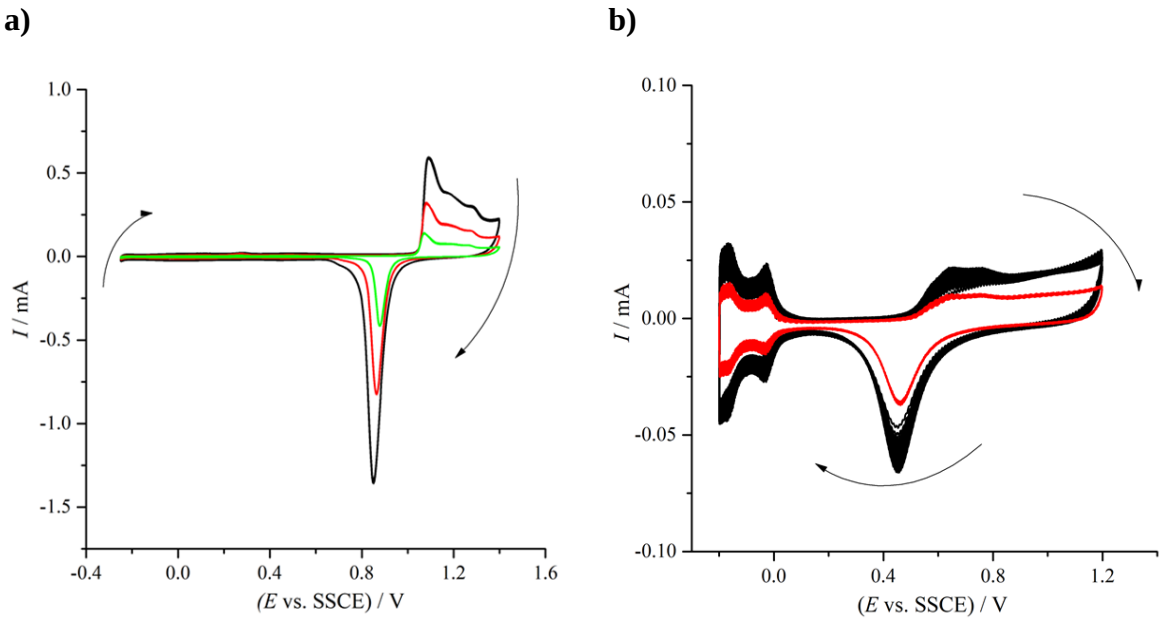

Fig. A1.: Electrochemical cleaning by cyclic voltammetry.
a) Cyclic voltammogram of the gold electrode "*2"* in 0.1 M H_2SO_4.
Potential range: (E = -0.25 – +1.4 V) vs. SSCE.
Scan rates: 100 (▬); 50 (▬) and 20 (▬) mV/s.
b) Cyclic voltammogram of the platinum rotating disk electrode "*5"* in 0.1 M H_2SO_4.
Potential range: (E = -0.2 – +1.2 V) vs. SSCE.
Scan rates: 100 (▬) and 50 (▬) mV/s.

A2 Potentials of reference electrodes

	(*E* vs. NHE) / V (at 25 °C)
SCE	0.2412
SSCE	0.2360

Table A1.: The electrode potencials of saturated calomel electrode (SCE) and sodium chloride saturated calomel electrode (SSCE).The potential values are against normal hydrogen electrode (NHE) at 25 °C. [68]

A3 Argand diagrams

Argand diagrams are plots of the minus one times the imaginary part of the impedance against the real part of the impedance. The axes of the Argand diagrams must be evenly scaled so that we can draw any conclusions from the shape of the curve.

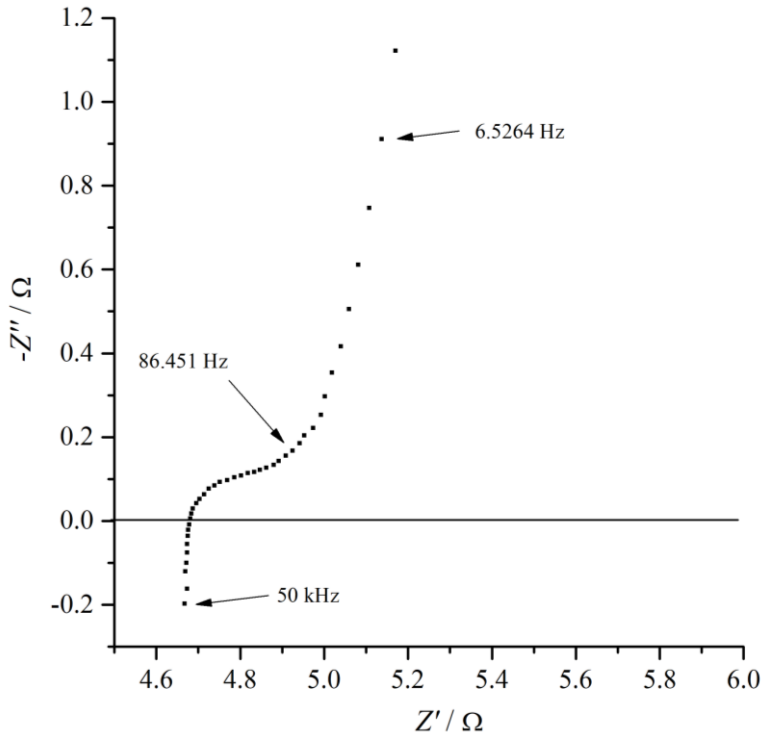

Fig. A2.: Uncorrected Argand diagram of the Au | PEDOT | Pd sample *Pd2*.
Recorded at the potential of *E* = 0.0 V vs. SSCE in 0.1 M H_2SO_4.
High frequency region of the curve.
Z ' and *Z* " denote the real and the imaginary parts of the impedance, respectively.

The imaginary part of the impedance must be corrected if the inductivity causes errors which cannot be considered negligible. The inductivity can be estimated using the following assumptions.

It is assumed that the magnitude of the impedance is negligible at sufficiently high frequencies. In this case, the admittance of an RC circuit (modeling the polymer-electrode system) can be expressed as following:

$$Y_{RC} = \frac{1}{Z_{RC}} = i\omega C_{dl} + \frac{1}{R_{ct}} = \frac{1 + i\omega R_{ct} C_{dl}}{R_{ct}} \quad \text{(A1)}$$

Thus, the impedance of the RC circuit can be expressed as following:

$$Z_{RC} = \frac{R_{ct}}{1 + i\omega R_{ct} C_{dl}} = \frac{R_{ct} - i\omega R_{ct}^2 C_{dl}}{1 + \omega^2 R_{ct}^2 C_{dl}^2} \quad \text{(A2)}$$

The RC circuit is connected in series with the inductivity (L) and the solution resistance (R_s), therefore the impedance of the whole circuit arises from the inductivity and the imaginary part of the impedance of the RC circuit:

$$Z'' = \omega L - \frac{\omega R_{ct}^2 C_{dl}}{1 + \omega^2 R_{ct}^2 C_{dl}^2} \quad \text{(A3)}$$

Multiplication by the denominator yields:

$$Z'' + Z''\omega^2 R_{ct}^2 C_{dl}^2 = \omega L + \omega^3 L R_{ct}^2 C_{dl}^2 - \omega R_{ct}^2 C_{dl} \quad \text{(A4)}$$

Division by ω^2 results in the following expression:

$$\frac{Z''}{\omega^2} + Z'' R_{ct}^2 C_{dl}^2 = \frac{L}{\omega} + \omega L R_{ct}^2 C_{dl}^2 - \frac{R_{ct}^2 C_{dl}}{\omega} \quad \text{(A5)}$$

In case of the studied electrodes, Z''/ω^2 is significantly smaller than $Z'' R_{ct}^2 C_{dl}^2$ at sufficiently high frequencies. Thus, discarding Z''/ω^2 and dividing by $\omega/R_{ct}^2 C_{dl}^2$ yields:

$$Z''\omega \approx \left(\frac{L}{R_{ct}^2 C_{dl}^2} - \frac{1}{C_{dl}}\right) + L\omega^2 \quad \text{(A6)}$$

Therefore, if $(Z''\omega)$ is plotted against (ω^2), the inductivity can be obtained from the linear fit in the high frequency range, as we can see in *Fig.A3.*

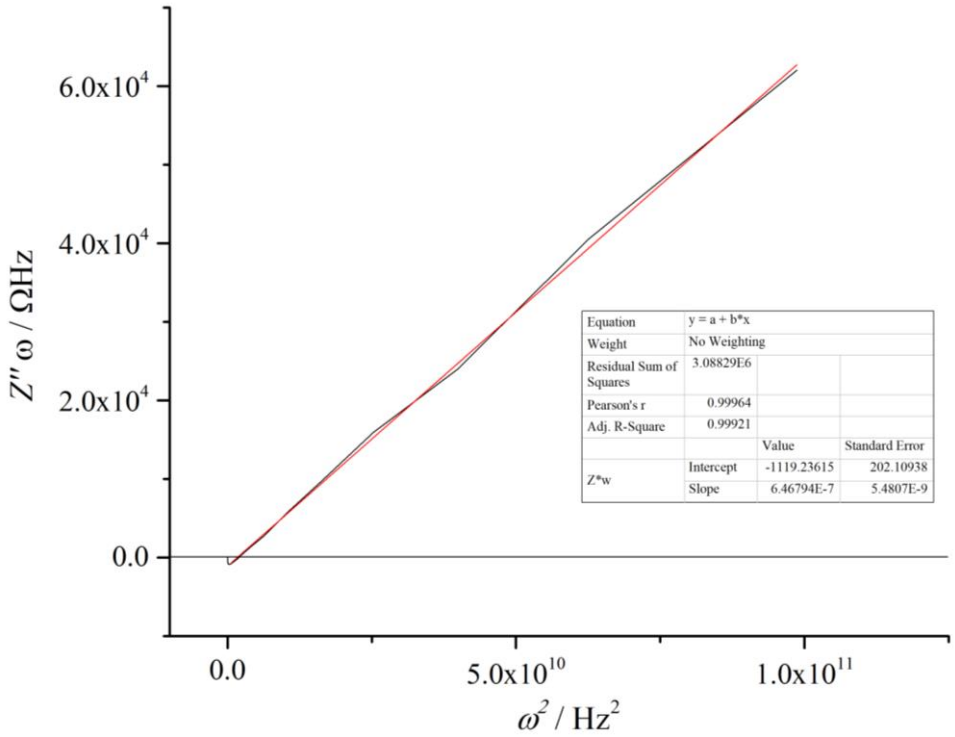

Fig. A3.: Correction of the inductivity in the impedance spectra of the Au | PEDOT | Pd sample *Pd2*.
Recorded at the potential of E = 0.0 V vs. SSCE in 0.1 M H_2SO_4.

Thus, the corrected value of the imaginary part of the impedance:

$$-Z'' \approx -Z'' + 2\pi f L \qquad \text{(A7)}$$

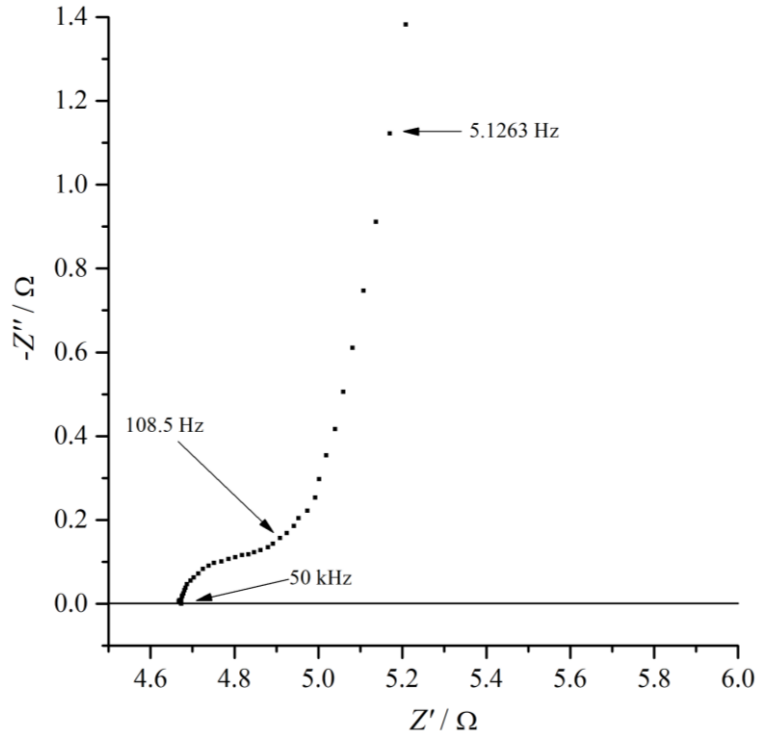

Fig. A4.: Argand diagram of the Au | PEDOT | Pd sample *Pd2*.
Recorded at the potential of E = 0.0 V vs. SSCE in 0.1 M H_2SO_4.
High frequency region of the curve.
Z' denotes the real part of the impedance, Z'' denotes the imaginary part of the impedance corrected by the inductivity.

A4 Admittance diagrams

Admittance diagrams are plots of the imaginary part of the admittance against the real part of the admittance. The axes of admittance diagrams must be evenly scaled so that we can draw any conclusions from the shape of the curve. The real part and the imaginary part of the admittance can be expressed as the following:

$$Y' = \frac{Z'}{|Z|^2} \tag{A8}$$

$$Y'' = \frac{-Z''}{|Z|^2} \tag{A9}$$

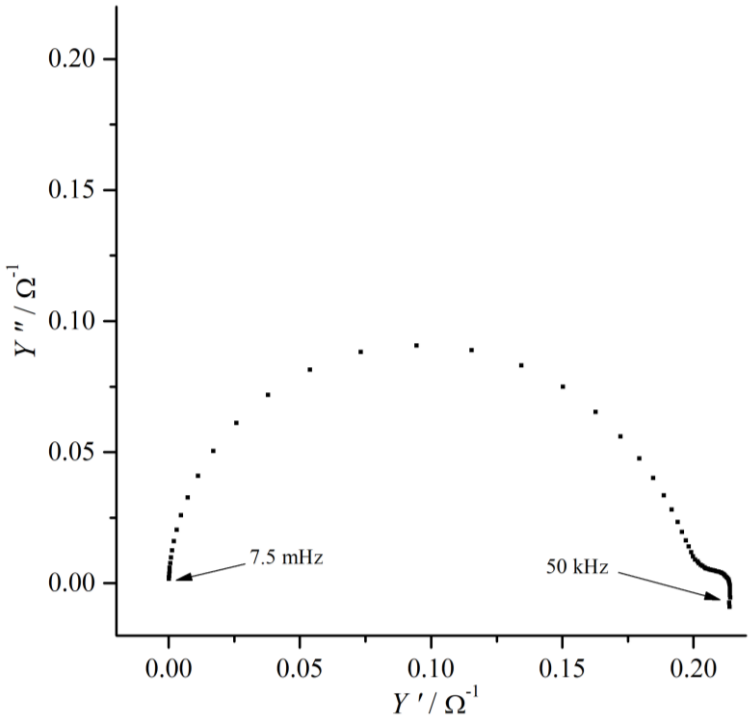

Fig. A5.: Admittance diagram of the Au | PEDOT | Pd sample *Pd2*.
Recorded at the potential of E = 0.0 V vs. SSCE in 0.1 M H_2SO_4.
The imaginary part (*Y''*) of the admittance as a function of the real part (*Y* ') of the admittance.

A5 Bode diagrams

Bode diagrams display the phase angle plotted against the logarithm of the frequency or the logarithm of the magnitude of the impedance plotted against the logarithm of the frequency. The representation of the phase angle and the magnitude of the impedance in the complex plane can be seen in *Fig.A5.*

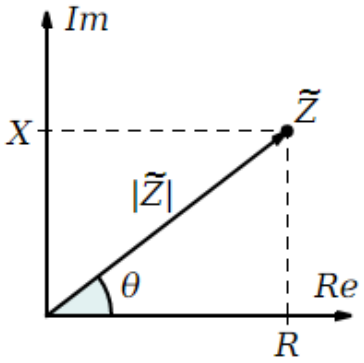

Fig. A6.: Representation of the phase angle and the magnitude of the impedance in the complex plane. [69]

The magnitude of the impedance ($|Z|$) can be expressed as the following:

$$|Z| = \sqrt{Z'^2 + Z''^2} \tag{A10}$$

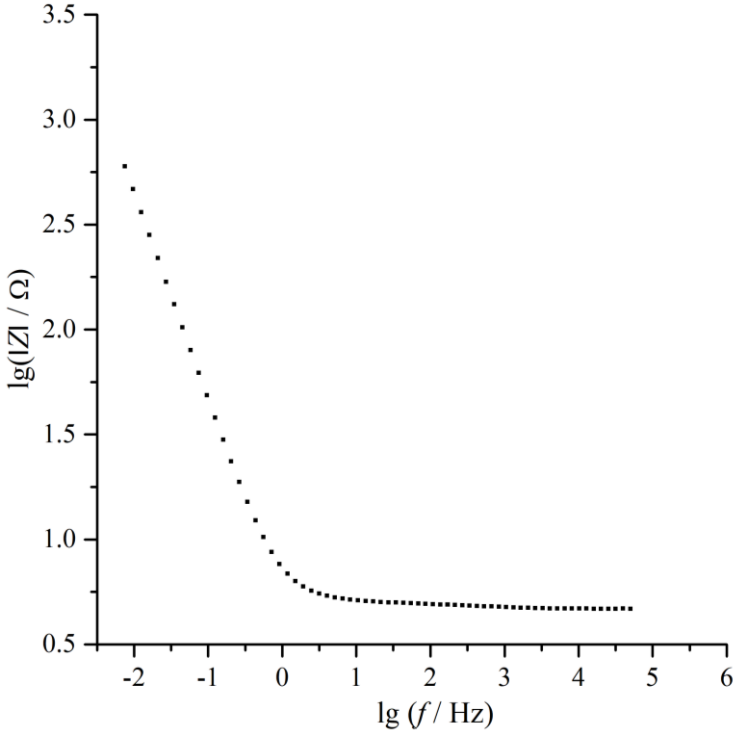

Fig. A7.: Bode diagram of the Au | PEDOT | Pd sample *Pd2*.
Recorded at the potential of E = 0.0 V vs. SSCE in 0.1 M H_2SO_4.
$\lg|\tilde{Z}|$ as a function of $\lg\tilde{f}$ ($|\tilde{Z}|$is the modulus of the impedance).
~ signs denote the magnitude of quantities.

The phase angle (φ) can be expressed by the following equation:

$$\varphi = cos^{-1}\frac{Z'}{|Z|} \tag{A11}$$

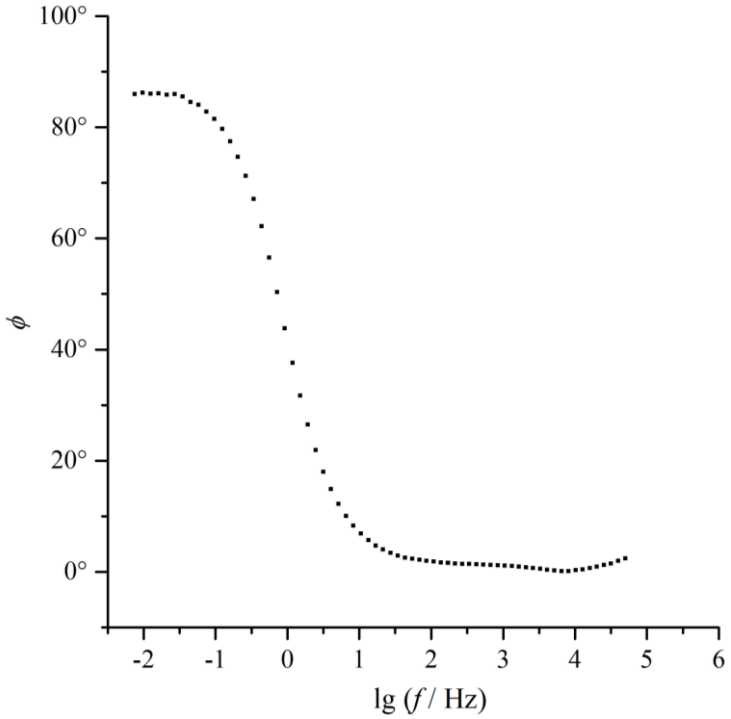

Fig. A8.: Bode diagram of the Au | PEDOT | Pd sample *Pd2*.
Recorded at the potential of E = 0.0 V vs. SSCE in 0.1 M H_2SO_4.
Phase angle as a function of lg$\tilde{f}$.
The ~ sign denotes the magnitude of the frequency.

A6 Graphic evaluation methods

Graphic evaluation methods result in estimated values which give us an impression of the characteristics of the studied system. Furthermore, estimated values may be required during the use of complex nonlinear least squares procedures to calculate parameters of higher reliability. The representation of the graphic evaluation methods is done according to [70].

As it has been mentioned earlier, an equivalent electrical circuit can be used to model the impedance of a polymer-electrode system. An equivalent circuit consisting of an RC circuit connected in series with the inductivity and the solution resistance can be seen in *Fig.A9*.

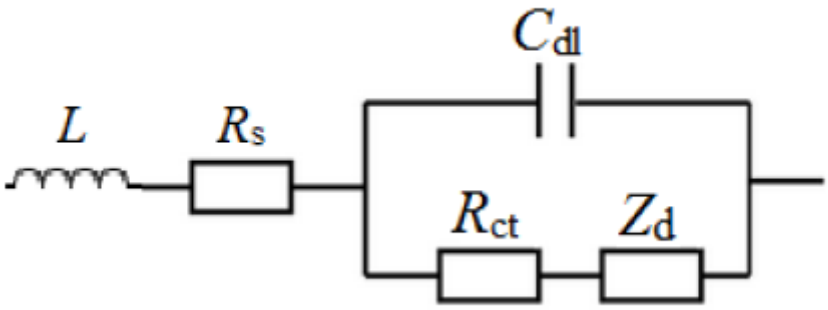

Fig. A9.: Randles-Erschler equivalent electrical circuit consisting of the inductivity (L), the solution resistance (R_s), the small frequency double layer capacity (C_{dl}), the charge transfer resistance (R_{ct}) and the Warburg impedance (Z_d). [70]

The graphical estimation of the solution resistance (R_s) and the charge transfer resistance (R_{ct}) can bee seen in *Fig.A10*.

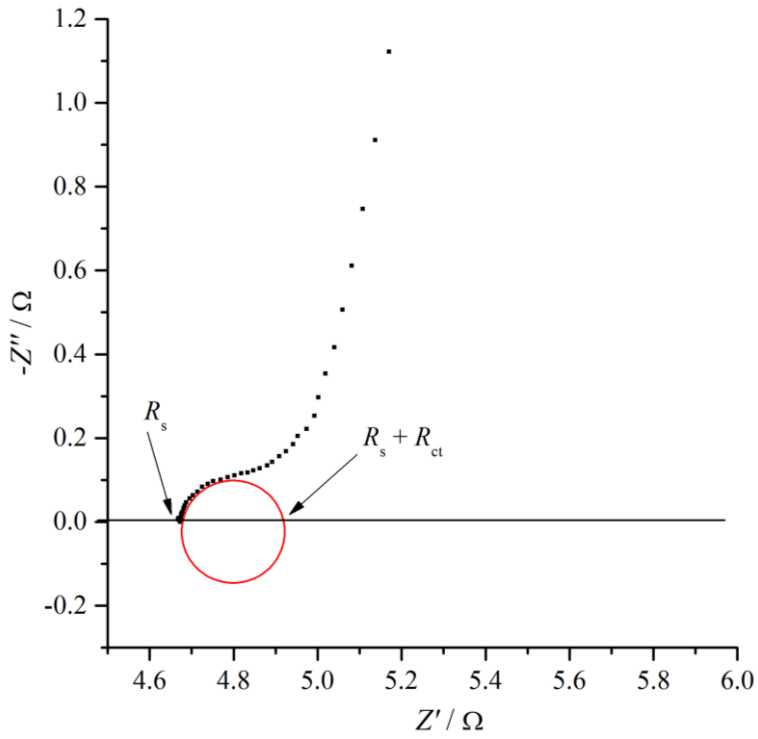

Fig. A10.: Graphical estimation of the solution resistance (R_s) and the charge transfer resistance (R_{ct}) in the Argand diagram of the Au | PEDOT | Pd sample *Pd2*.
Recorded at the potential of E = 0.0 V vs. SSCE in 0.1 M H_2SO_4.
High frequency region of the curve.
Z ' denotes the real part of the impedance, *Z ''* denotes the imaginary part of the impedance corrected by the inductivity.

The Warburg impedance element of the Randles-Erschler equivalent circuit describes the diffusion of the electrochemically active species within the polymer film. It dominates the electrochemical response of the system at medium frequencies and it can be estimated by the following relation:

$$-Z'' \approx \sigma\omega^{-1/2} \tag{A12}$$

The Warburg constant can be estimated by the slope of the linear fit in the medium frequency range of the $-Z''$ vs. $\omega^{-1/2}$ plot [71]. The determination of the Warburg constant can be seen in *Fig.A11.*

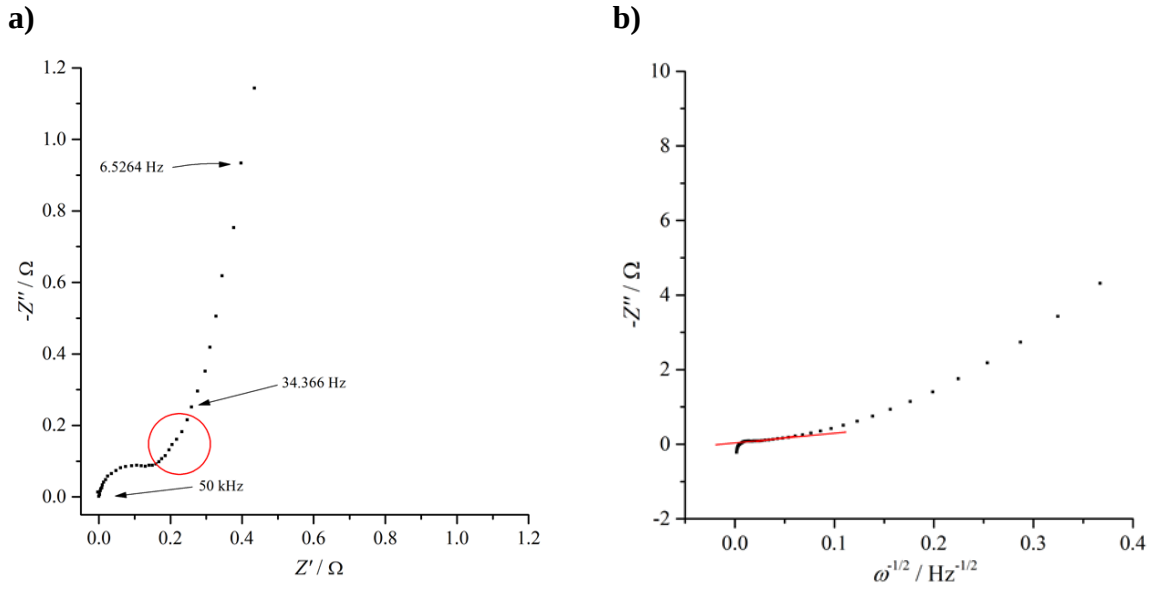

Fig. A11.: Determination of the Warburg contstant (σ) of the Au | PEDOT | Pd sample *Pd3* at the potential of E = 0.0 V vs. SSCE in 0.1 M H_2SO_4.
a) Warburg section in the Argand diagram of the Au | PEDOT | Pd sample *Pd3*.
b) Estimation of the Warburg constant by the linear fit in the medium frequency range of the -Z '' vs. $\omega^{-1/2}$ plot.

The small frequency double layer capacity of the studied system can be estimated by plotting the logarithm of the quotient of the admittance and the angular frequency against the logarithm of the frequency (see *Fig.A12.*).

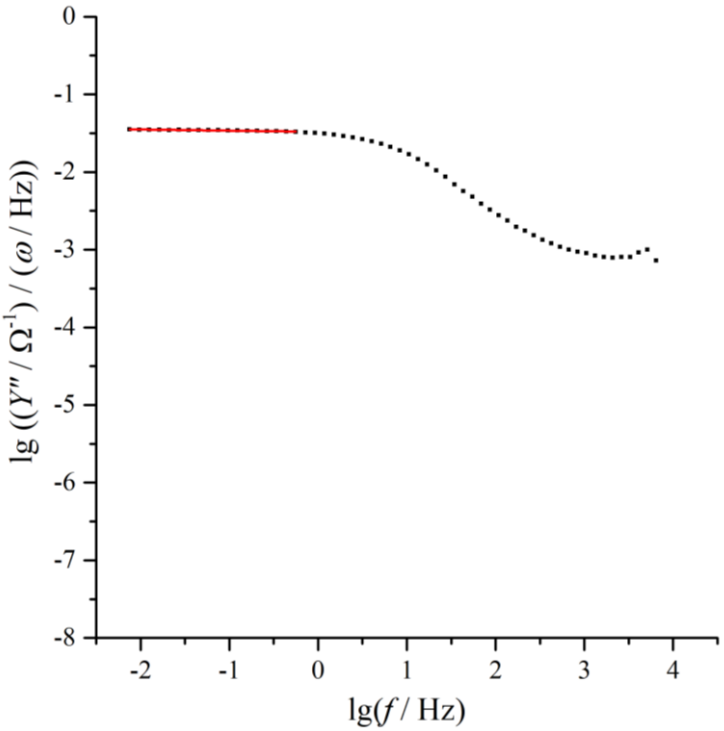

Fig. A12.: Determination of the small frequency double layer capacity (C_{dl}) of the Au | PEDOT | Pd sample *Pd2* at the potential of E = 0.0 V vs. SSCE in 0.1 M H_2SO_4.
lg (Y '' / ω) as a function of lg$\tilde{f}$.
The ~ sign denotes the magnitude of the frequency.

The small frequency range of the spectrum can be described by a constant phase element whose impedance can be expressed as the following:

$$Z = \frac{1}{B}\,(i\omega)^{-\alpha} \qquad \text{(A13)}$$

In the equation (A13) α is an empirical constant with the following ideal cases: α = 0 in case of pure ohmic resistance, α = 1 in case of a condensator, α = -1 in case of pure inductivity and α = 1/2 in case of Warburg impedance. The admittance of the equation (A13) can be expressed as the following:

$$Y = B\ (i\omega)^{\alpha} \tag{A14}$$

The equation (A14) can be converted into a trigonometric form:

$$Y = B\ \omega^{\alpha}\left(\cos\left(\frac{\alpha\pi}{2}\right) + i\ \sin\left(\frac{\alpha\pi}{2}\right)\right) \tag{A15}$$

Dividing the imaginary part of the admittance by the angular frequency yields:

$$\frac{Y''}{\omega} = B\omega^{\alpha-1}\sin\left(\frac{\alpha\pi}{2}\right) \tag{A15}$$

Using that $\omega = 2\pi f$, the logarithm of the equation (A15) can be expressed as the following:

$$\lg\left(\frac{Y''}{\omega}\right) = (\alpha - 1)\lg(2\pi) + (\alpha - 1)\lg f + \lg B + \lg\left(\sin\left(\frac{\alpha\pi}{2}\right)\right) \tag{A16}$$

If the left side of the equation (A16) is plotted against the logarithm of the frequency, we'll find the factor of $\lg f$ to be zero in case of a condensator ($\alpha = 1$). Thus, the slope of the curve will be approximately zero in the small frequency region of the curve (see *Fig. A12.*). A linear fit in this range of the curve will yield the value of (α - 1). By the use of the value of α and the intercept of the linear fit, B (the value of the small frequency double layer capacity) can be obtained.

A7 Determination of the limiting currents for the Levich plot

To be able to determine the limiting currents for the Levich plot of the composite, the anodic capacitive current must be corrected for. The anodic capacitive current is estimated based on the voltammogram recorded in argon saturated solution (see *Fig. A13*). The voltammograms recorded in air saturated solution are corrected by subtracting the estimated value of the anodic capacitive current. The corrected voltammograms with the spots for the determination of the limiting currents can be seen in *Fig. A13*.

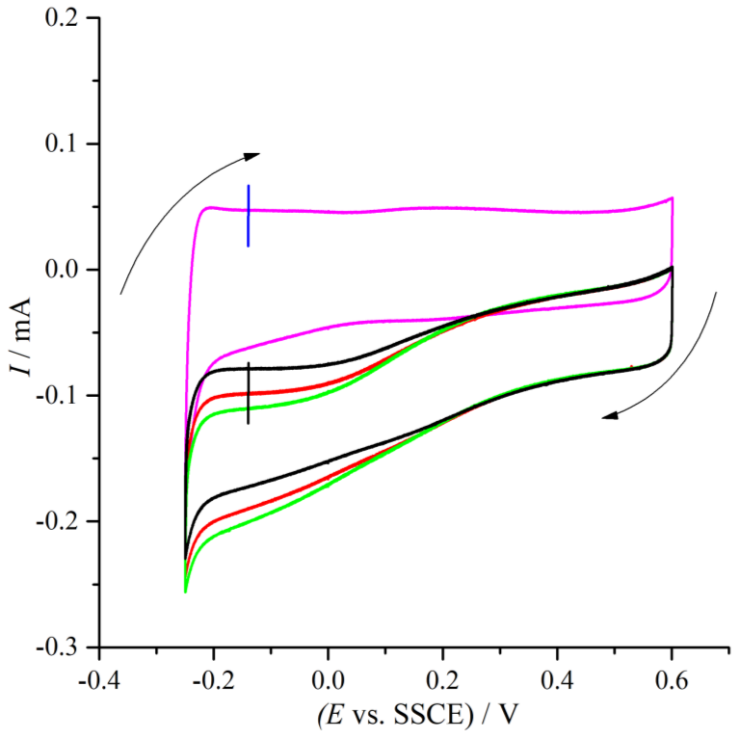

Fig. A13.: Determination of the limiting currents in the corrected voltammograms of the Pt | PEDOT | Pt sample *Pt5*.
Recorded in 0.1 M H_2SO_4 saturated with air.
Potential range: (E = -0.25 – +0.6 V) vs. SSCE.
Scan rates: 10 mV/s in argon saturated solution ( ); 10 mV/s in air saturated solution at 500 rpm ( ), 1000 rpm ( ) and 1500 rpm ( ).
The anodic capacitive current was estimated at the potential of E = -0.143 V vs. SSCE (marked by a blue line).
The limiting currents were determined at the same potential (E = -0.143 V vs. SSCE, marked by a black line).

References

[1] C. K. Chiang, C. R. J. Fincher, Y. W. Park, A. J. Heeger, H. Shirakawa, E. J. Louis, S. C. Gau and A. G. MacDiarmid, "Electrical Conductivity in Doped Polyacetylene," *Physical Review Letters* , vol. 39, no. 17, pp. 1098-1101, 1977.

[2] W. Lövenich, "PEDOT- Properties and applications," 2014.

[3] H.Letheby, "On the production of a blue substance by the electrolysis of sulphate of aniline," *Journal of the Chemical Society XV.,* pp. 161-163, 1862.

[4] I. Mamadou, L. Yu and R. Buvet, "Conductivity of polyaniline and polypyrrole composites under point-plane geometry electronic injection," *Compt. Rend.C* , vol. 279, no. 23, pp. 931-934, 1974.

[5] M. Armour, A. G. Davies and A. W. J. Upadhyay, "Colored Electrically Conducting Polymers from Furan, Pyrrole and Thiophene," *Journal of Polymer Science A-1, vol. 5,* pp. 1527-1538, 1967.

[6] G. Tourillon and F. Garnier, "New electrochemically generated organic conducting polymers," *Journal of Electroanalytical Chemistry and Interfacial Electrochemistry* , vol. 135, no. 1, pp. 173-178, 1982.

[7] A. Elschner, S. Kirschmeyer, W. Lövenich, U. Merker and K. Reuter, PEDOT: Principles and applications of an intrinsically conductive polymer, 2010.

[8] G. Inzelt, Conducting Polymers - A New Era in Electrochemistry, Berlin: Springer, 2008.

[9] L. G. -. Mobarakeh, M. Prabhakaran, M. Morshed, M. Nasr-Esfahani, H. Baharvand, S. Kiani, S. Al-Deyab and S. Ramakrishna, "Application of conductive polymers, scaffolds and electrical stimulation for nerve tissue engineering," *Journal of Tissue Engineering and Regenerative Medicine* , vol. 5, no. 4, pp. 17-35, 2011.

[10] N. K. Guimard, N. Gomez and C. E. Schmidt, "Conducting polymers in biomedical engineering," *Progress in Polymer Science* , vol. 32, no. 8-9, pp. 876-921, 2007.

[11] B. Lakard, L. Ploux, K. Anselme, F. Lallemand, S. Lakard, M. Nardin and J. Hihn, "Effect of ultrasounds on the electrochemical synthesis of polypyrrole, application to the adhesion and growth of biological cells," *Bioelectrochemistry* , vol. 75, no. 2, pp. 148-157, 2009.

[12] A. Kotwal and C. E. Schmidt, "Electrical stimulation alters protein adsorption and nerve cell interactions with electrically conducting biomaterials," *Biomaterials* , vol. 22, no. 10, pp. 1055-1064, 2001.

[13] J. Y. Lee, C. A. Bashur, A. S. Goldstein and C. E. Schmidt, “Polypyrrole-Coated Electrospun PLGA Nanofibers for Neural Tissue Applications,” *Biomaterials* , vol. 30, no. 26, pp. 4325-4335, 2009.

[14] G. G. Wallace, M. Smyth and H. Zhao, “Conducting electroactive polymer-based biosensors,” *Trends of Analytic Chemistry vol.18 issue 4,* vol. 18, no. 4, pp. 245-251, 1999.

[15] R. Balint, N. J. Cassidy and S. H. Cartmell, “Conductive polymers: Towards a smart biomaterial for tissue engineering,” *Acta Biomaterialia ,* vol. 10, no. 6, pp. 2341-2353, 2014.

[16] “www.labspaces.net,” [Online].

[17] E. G. Tolstopyatova, N. A. Pogulaichenko, S. N. Eliseeva and V. V. Kondratiev, “Spectroelectrochemical study of poly-3,4-ethylenedioxythiophene films in the presence of different supporting electrolytes,” *Russian Journal of Electrochemistry,* vol. 45, no. 3, p. 252, 2009.

[18] X. Crispin, F. L. E. Jakobsson, A. Crispin, P. C. M. Grim, P. Andersson, A. Volodin, C. v. Haesendonck, M. V. d. Auweraer, W. R. Salaneck and M. Berggren, “The Origin of the High Conductivity of Poly(3,4-ethylenedioxythiophene)−Poly(styrenesulfonate) (PEDOT−PSS) Plastic Electrodes,” *Chemistry of Materials* , vol. 18, no. 18, pp. 4354-4360, 2006.

[19] J. Li and Y. Ma, “In-situ synthesis of transparent conductive PEDOT coating on PET foil by liquid phase depositional polymerization of EDOT,” *Synthetic Metals* , vol. 217, pp. 185-188, 2016.

[20] T. Takano, H. Masunaga, A. Fujiwara, H. Okuzaki and T. Sasaki, “PEDOT nanocrystal in highly conductive PEDOT:PSS polymer films,” *Macromolecules,* vol. 45, no. 9, pp. 3859-3865, 2012.

[21] G. Chen, R. Rodriguez, L. Fei, Y. Xu, S. Deng, S. Smirnov and H. Luo, “A facile hydrothermal route to iron(III) oxide with conductive additives as composite anode for lithium ion batteries,” *Journal of Power Sources vol. 259,* pp. 227-232, 2014.

[22] E. K. Park, M. Choi, J.-H. Jeun, K.-T. Lim, J.-M. Kim and Y.-S. Kim, “The effect of metal oxide nanoparticle concentrations in PEDOT:PSS layer on the performance of P3HT:PCBM organic solar cells,” *Microelectronic Engineering* , vol. 111, pp. 166-169, 2013.

[23] J. Kim, E. Kim, Y. Won, H. Lee and K. Suh, “The preparation and characteristics of conductive poly(3,4-ethylenedioxythiophene) thin film by vapor-phase polymerization,” *Synthetic Metals* , vol. 139, no. 2, pp. 485-489, 2003.

[24] S. Y. Kim, M. S. Cho, J. D. Nam and Y. Lee, “Transparent and Conductive PEDOT Films on PET Substrate Using an Epoxy Acrylate Binder,” *Key Engineering Materials* , Vols. 326-328, pp. 1519-1522, 2006.

[25] V. Castagnola, C. Bayon, E. Descamps and C. Bergaud, “Morphology and conductivity of PEDOT layers produced by different electrochemical routes,” *Synthetic Metals,* vol. 189, pp. 7-16, 2014.

[26] S. Patra, K. Barai and N. Munichandraiah, “Scanning electrode microscopy studies of PEDOT prepared by various electrochemical routes,” *Synthetic Metals,* vol. 158, pp. 430-435, 2008.

[27] A.J.Epstein, “Insulator-metal transition and transition and metallic state in conducting polymers,” in *Handbook of Conducting Polymers,* Boca Raton, CRC Press, 2007.

[28] K. E. Aasmundtveit, E. J. Samuelsen, L. A. A. Pettersson, O. Inganäs, T. Johansson and R. Feidenhans'l, “Structure of thin films of poly(3,4-ethylenedioxythiophene),” *Synthetic Metals ,* vol. 101, no. 1-3, pp. 561-564, 1999.

[29] F. Jonas and G. Heywang.Patent DE Patent No. 3813589, 1988.

[30] A. M. Smolin, M. P. Novoselov, T. A. Babkova, S. N. Eliseeva and V. V. Kondratiev, “Use of Composite Films Based on Poly(3,4Ethylenedioxythiophene) with Inclusions of Palladium Nanoparticles in Voltammetric Sensors for Hydrogen Peroxide,” *Journal of Analytical Chemistry ,* vol. 70, no. 8, pp. 967-973, 2015.

[31] F. Jiang, R. Yue, Y. Du, J. Xu and P. Yang, “A one-pot ‘green’ synthesis of Pd-decorated PEDOT nanospheres for nonenzymatic hydrogen peroxide sensing,” *BIosensors and Bioelectronics vol. 44,* pp. 127-131, 2013.

[32] E. G. Tolstopjatova, V. V. Kondratiev and S. N. Eliseeva, “Multi-layer PEDOT:PSS/Pd composite electrodes for hydrazine oxidation,” *Journal of Solid State Electrochemistry ,* vol. 19, pp. 2951-2959, 2015.

[33] F. Jiang, Z. Yao, R. Yue, J. Xu, Y. Du, P.Yang and C. Wang, “Electrocatalytic activity of Pd nanoparticles supported on poly(3,4-ethylenedioxythiophene)-graphene hybrid for ethanol electrooxidation,” *Journal of Solid State Electrochemistry ,* vol. 17, no. 4, pp. 1039-1047, 2013.

[34] S. Dash and N. Munichandraiah, “Electrocatalytic oxidation of 1,2-propanediol on electrodeposited Pd–poly(3,4-ethylenedioxythiophene) nanodendrite films in alkaline medium,” *Electrochimica Acta ,* vol. 80, pp. 68-76, 2012.

[35] H. Hosseini, S. J. T. Rezaei, P. Rahmani, R. Sharifi, M. R. Nabid and A. Bagheri, “Nonenzymatic glucose and hydrogen peroxide sensors based on catalytic properties of palladium nanoparticles / poly(3,4-ethylenedioxythiophene) nanofibers,” *Sensors and actuators B: Chemical ,* vol. 195, pp. 85-91, 2014.

[36] P. Santhosh, K. M. Manesh, S. Uthayakumar, S. Komathi, A. I. Gopalan and K.-P. Lee, “Fabrication of enzymatic glucose biosensor based on palladium nanoparticles dispersed onto poly(3,4-ethylenedioxythiophene) nanofibers,” *Bioelectrochemistry,* vol. 75, pp. 61-66, 2009.

[37] K. Yin and Z. Zhu, “"One-pot" synthesis, characterization, and NH3-sensing of Pd/PEDOT:PSS nanocomposite,” *Synthetic Metals,* vol. 160, pp. 1115-1118, 2010.

[38] J. E. Choe, M. S. Ahmed and S. Jeon, “3,4-Ethylenedioxythiophene functionalized graphene with palladium nanoparticles for enhanced electrocatalytic oxygen reduction reaction,” *Journal of Power Sources,* vol. 281, pp. 211-218, 2015.

[39] V. V. Kondratiev, T. A. Babkova and E. G. Tolstopjatova, “PEDOT-supported Pd nanoparticles as a catalyst for hydrazine oxidation,” *Journal of Solid State Electrochemistry,* vol. 17, pp. 1621-1630, 2013.

[40] Z. Zhang, J. Zhang, H. Zhang, J. Xu, Y. Wen and W. Ding, “Characterization of PEDOT:PSS-reduced graphene oxide@Pd composite electrode and its application in voltammetric determination of vitamin K3,” *Journal of Electroanalytical Chemistry,* vol. 775, pp. 258-266, 2016.

[41] V. V. Kondratiev, T. A. Babkova and S. N. Eliseeva, “Structure and electrochemical properties of composite films based on poly-3,4-Ethylenedioxythiophene with metallic palladium inclusions,” *Russian Journal of Electrochemistry,* vol. 48, no. 2, pp. 205-211, 2012.

[42] S. Harish, J. Mathiyarasu, K. L. N. Phani and V. Yegnaraman, “Synthesis of Conducting Polymer Supported Pd Nanoparticles in Aqueous Medium and Catalytic Activity Towards 4-Nitrophenol Reduction,” *Catal. Lett.,* vol. 128, pp. 197-202, 2009.

[43] S. N. Eliseeva, V. V. Malev and V. V. Kondratiev, “Electrochemical Properties of Composite Films Based on Poly-3,4-Ethylenedioxythiophene with Inclusions of Metallic Palladium,” *Russian Journal of Electrochemistry,* vol. 45, no. 9, pp. 1045-1051, 2009.

[44] M. Ilieva, A. Nakova and V. Tsakova, “Pd-modified Pedot layers obtained through electroless metal deposition - electrooxidation of glycerol,” *Journal of Solid State Electrochemistry,* vol. 20, pp. 3015-3023, 2016.

[45] T. A. Babkova, V. V. Kondratiev and D. I. Shevaldysheva, “Oxidation of Hydrazine on Poly-3,4-Ethylenedioxythiophene Polymer Films with Inclusions of Palladium Nanoparticles,” *Russian Journal of Electrochemistry,* vol. 49, no. 3, pp. 259-264, 2013.

[46] S. N. Eliseeva, E. V. Ubyivovk, A. S. Bondarenko, O. F. Vyvenko and V. V. Kondratiev, “Synthesis and Structure of Poly(3,4-ethylenedioxythiophene) Film with the Inclusions of Palladium Nanoparticles,” *Russian Journal of General Chemistry,* vol. 80, no. 6, pp. 1143-1148, 2010.

[47] S. Harish, J. Mathiyarashu, K. L. N. Phani and V. Yegnaraman, “PEDOT/Palladium composite material: synthesis, characterization and application to simultaneous determination of dopamine and uric acid,” *Journal of Applied Electrochemistry,* vol. 38, pp. 1583-1588, 2008.

[48] S. Dash and N. Munichandraiah, “Nanoflowers of PdRu on PEDOT for Electrooxidation of Glycerol and Its Analysis,” *Electrochimica Acta,* vol. 180, pp. 339-352, 2015.

[49] K. K. Tintula, S. Pitchumani, P. Sridhar and A. K. Shukla, “A solid-polymer-electrolyte direct methanol fuel cell (DMFC) with Pt-Ru nanoparticles supported onto poly(3,4-ethylenedioxythiophene) and polystyrene sulfonic acid polymer composite as anode,” *Journal of Chemical Sciences,* vol. 122, no. 3, pp. 381-389, 2010.

[50] J.-F. Drillet, R. Dittmeyer and K. Jüttner, “Activity and long-term stability of PEDOT as Pt catalyst support for the DMFC anode,” *Journal of Applied Electrochemistry,* vol. 37, pp. 1219-1226, 2007.

[51] T. -H. Tsai, C.-Y. Yang and S.-M. Chen, “Efficiency Enhancement with Electrodeposited Pt-Ru Bimetallic Nanoparticles and Poly(3,4-ethylenedioxythiophene) Hybrid Film as Counter ELectrode in Dye-Sensitized Solar Cells,” *International Journal of Electrochemical Science,* vol. 7, pp. 12764-12773, 2012.

[52] S. Dash, S. Patra and N. Munichandraiah, “Electrooxidation of Formic Acid at Platinum Nanoclusters Electrodeposited on PEDOT Coated Carbon Paper Electrode,” *Journal of Applied Electrochemistry,* vol. 42, pp. 59-67, 2012.

[53] M. A. d. Valle, R. Salgado and F. Armijo, “PEDOT Nanowires and Platinum Nanoparticles Modified Electrodes to be Assayed in Formic Acid Electro-oxidation,” *International Journal of Electrochemical Science,* vol. 9, pp. 1557-1564, 2014.

[54] L.-C. Chang, H.-N. Wu, C.-Y. Lin, Y.-H. Lai, C.-W. Hu and K.-C. Ho, “One-pot Synthesis of Poly(3,4-ethylenedioxythiophene) - Pt Nanoparticle Composite and Its Application to Electrochemical H2O2 Sensor,” *Nanoscale Research Letters,* vol. 7, p. 319, 2012.

[55] T.-Y. Wu, Z.-Y. Kuo, J. J.-J, C.-W. Kuo, C.-J. Tsai, P.-R. Chen and H.-R. Chen, “Co-electrodeposition of Platinum and Rhodium in Poly(3,4-ethylenedioxythiophene)-Poly(styrenesulfonic acid) as Electrocatalyst for Methanol Oxidation,” *International Journal of Electrochemical Science,* vol. 7, pp. 8076-8090, 2012.

[56] S. Patra and N. Munichandraiah, “Electrooxidation of Methanol on Pt-modified Conductive Polymer PEDOT,” *Langmuir,* vol. 25, pp. 1732-1738, 2009.

[57] R. Yue, Z. Yao, J. Geng, Y. Du, J. Xu and P. Yang, “Facile Electrochemical Synthesis of a Conducting Copolymer from 5-aminoindole and EDOT and Its Use as Pt Catalyst Support for Formic Acid Electrooxidation,” *Journal of Solid State Electrochemistry,* vol. 17, pp. 751-760, 2013.

[58] X. L. Tian, Y. Y. Xu, W. Zhang, T. Wu, B. Y. Xia and X. Wang, “Unsupported Platinum-Based Electrocatalysts for Oxygen Reduction Reaction,” *ACS Energy Letters,* vol. 2, pp. 2035-2043, 2017.

[59] V. T. T. Ho, C.-J. Pan, J. Rick, W.-N. Su and B.-J. Hwang, "Nanostructured Ti0,7Mo0,3O2 Support Enhances Electron Transfer to Platinum: High Performance Catalyst for Oxygen Reduction Reaction," *Journal of the American Chemical Society,* vol. 133, no. 30, pp. 11716-11724, 2011.

[60] S. M. Alia, G. Zhang, D. Kisailus, D. Li, S. Gu, K. Jensen and Y. Yan, "Porous Platinum Nanotubes for Oxygen Reduction and Methanol Oxidation Reactions," *Advanced Functional Materials,* vol. 20, no. 21, pp. 3742-3746, 2010.

[61] J. Kim, U.-S. Im, D.-H. Peck, S.-H. Yoon, H.-S. Park and D.-H. Jung, "Enhanced Activity and Durability of the Oxygen Reduction Catalysts Supported on the Surface Expanded Tubular-Type Carbon Nanofiber," *Applied Catalysis B: Environmental,* vol. 217, pp. 192-200, 2017.

[62] F. E. S. Oztuna, S. B. Barim, S. E. Bozbag, H. Yu, M. Aindow, U. Unal and C. Erkey, "Graphene Aerogel Supported Platinum Electrocatalysts for Oxygen Reduction Reaction by Supercritical Deposition," *Electrochimica Acta,* vol. 250, pp. 174-184, 2017.

[63] G. Inzelt, in *Conducting Polymers - A New Era in Electrochemistry*, Berlin, Springer, 2008, pp. 68-71.

[64] G. Inzelt, in *Az elektrokémia korszerű elmélete és módszerei, I.*, Budapest, Nemzeti Tankönyvkiadó, 1999.

[65] G. Inzelt, in *Conducting Polymers - A New Era in Electrochemistry*, Berlin, Springer , 2008, pp. 72-74.

[66] G. Inzelt, in *Conducting Polymers - A New Era in Electrochemistry*, Berlin, Springer, 2008, p. 77.

[67] J. Goldstein, D. Newbury, D. Joy, A. Romig, C. Lyman, C. Fiori and E. Lifshin, Scanning electron microscopy and X-ray microanalysis, New York: Plenum, 1992.

[68] A. Bard, L. Faulkner and J. Wiley, Electrochemical Methods: Fundamentals and Applications, New York, 2000.

[69] "Wikimedia Commons," 2017. [Online]. Available: https://commons.wikimedia.org/wiki/File:Complex_Impedance.svg.

[70] K. J. Szekeres, *Kapcsolat vezető polimer-filmek elektrokémiai viselkedése és morfológiája között, MSc thesis,* Budapest, 2017.

[71] G. Inzelt and G. Láng, "Electropolymerization," in *Electrochemical Impedance Spectroscopy (EIS) for Polymer Characterization*, 2010.